The Seismicity Rate Model for the 2022 Aotearoa New Zealand National Seismic Hazard Model

Matthew C. Gerstenberger* *et al.*

ABSTRACT

A seismicity rate model (SRM) has been developed as part of the 2022 Aotearoa New Zealand National Seismic Hazard Model revision. The SRM consists of many component models, each of which falls into one of two classes: (1) inversion fault model (IFM); or (2) distributed seismicity model (DSM). Here we provide an overview of the SRM and a brief description of each of the component models. The upper plate IFM forecasts the occurrence rate for hundreds of thousands of potential ruptures derived from the New Zealand Community Fault Model version 1.0 and utilizing either geologic- or geodetic-based fault-slip rates. These ruptures are typically less than a couple of hundred kilometers long, but can exceed 1500 km and extend along most of the length of the country (albeit with very low probabilities of exceedance [PoE]). We have also applied the IFM method to the two subduction zones of New Zealand and forecast earthquake magnitudes of up to $\sim M_w$ 9.4, again with very low PoE. The DSM combines a hybrid model developed using multiple datasets with a non-Poisson uniform rate zone model for lower seismicity regions of New Zealand. Forecasts for 100 yr are derived that account for overdispersion of the rate variability when compared with Poisson. Finally, the epistemic uncertainty has been modeled via the range of models and parameters implemented in an SRM logic tree. Results are presented, which indicate the sensitivity of hazard results to the logic tree branches and that were used to reduce the overall complexity of the logic tree.

KEY POINTS

- We update the seismicity rate model (SRM; earthquake rupture forecast) for the Aotearoa New Zealand National Seismic Hazard Model (NZ NSHM).
- An inversion fault model (IFM) method is applied to crustal faults and two subduction interfaces.
- The results provide a 100 year forecast, including epistemic uncertainty and non-Poisson variabilty.

Supplemental Material

INTRODUCTION

Gerstenberger, Bora, *et al.* (2022; Gerstenberger *et al.*, 2024) introduce a 2022 revision of the New Zealand National Seismic Hazard Model–Te Tauira Matapae Pūmate Rū i Aotearoa (NZ NSHM 2022). This was a major revision and introduced a fundamental redevelopment of all components of the model. Here we provide a high-level overview of the seismicity rate model (SRM) component of the NZ NSHM 2022 (Gerstenberger, Van Dissen, *et al.*, 2022). This overview is a companion to the ground-motion characterization model (GMCM) overview (Bradley *et al.*, 2022, 2024). Here we summarize the numerous component models and datasets of the SRM, most of which are described in detail in additional publications within the seismic hazard-focused *Seismological Research Letters* special focus sections and *Bulletin of the Seismological Society of America* special issue or in other various publications as shown in table 1 of Gerstenberger *et al.* (2024); also described is the philosophy and framework of the SRM. A central part of this is the development of an inversion-based model for the determination of rupture rates on the fault model (e.g., Field *et al.*, 2013, 2014; Page *et al.*, 2013).

Here, we lay out the basic structure of the article to help guide the reader. The Introduction section and Model Concept and Construction section describe the overarching philosophies and design of the model. Next is the SRM Dataset Curation and Underpinning Models section, which introduces aspects of the SRM that are critical to its construction but are a step removed from the core NSHM-specific modeling. The four sections that follow work together to provide an overview of the three primary component model groups that, together, form

Full author list and affiliations appear at the end of this article.

*Corresponding author: m.gerstenberger@gns.cri.nz

Cite this article as Gerstenberger, M. C., R. Van Dissen, C. Rollins, C. DiCaprio, K. KS. Thingbaijim, S. Bora, C. Chamberlain, A. Christophersen, G. L. Coffey, S. M. Ellis, *et al.* (2024). The Seismicity Rate Model for the 2022 Aotearoa New Zealand National Seismic Hazard Model, *Bull. Seismol. Soc. Am.* **XX**, 1–35, doi: 10.1785/0120230165

TABLE 1
Some Other Key Differences from the (Stirling *et al.*, 2002, 2012) Seismicity Rate Models (SRMs) with a Focus on Characterization of Epistemic Uncertainty

2002 and 2010 SRM	2022 SRM
Crustal fault earthquake ruptures	
~900 explicitly modeled crustal fault earthquake sources	Many thousands of explicitly modeled crustal fault earthquake sources
No magnitude uncertainty on sources	Wide range of magnitudes considered per source
Segmented fault ruptures: single magnitude rupture per fault source	Multifault complex ruptures and many ruptures of many magnitudes per fault source
Single model of slip rates on faults	Multiple models of slip rates on faults with both geologic and geodetic constraint
Hikurangi subduction interface earthquake sources	
Hikurangi subduction interface characterized by seven simple earthquake sources with the largest terminating at East Cape	Hikurangi subduction interface extended north to the Louisville Ridge to include Kermadec interface and now encompasses thousands of earthquake sources
Distributed seismicity sources	
Single smoothed seismicity model based on earthquake catalog (M_L)	Combination of many models informed by earthquake catalog (M_w), geodesy and geology; long-term clustering incorporated
Single model of variability in rate of occurrence	Two models of variability in rate of occurrence, one with increased variability for low-seismicity regions
Overall model considerations and philosophy	
Single occurrence rate forecast, and no consideration of epistemic uncertainty	Multiple occurrence rate forecasts, and characterization of epistemic uncertainty was a key consideration
Overall earthquake rate was an output (with no uncertainty)	Overall earthquake rate is a constraining input (with multiple models considered)
Single geological estimate of slip rate controlled overall all rate of large earthquakes	Multiple datasets and constraints used to inform a potential range of rate of large earthquakes (uncertainty in data and rate)
Nominally a long-term forecast with no consideration given of uncertainty arising from nonstationarity of seismicity	Nominally a forecast for the next century with consideration given to uncertainty that may arise from nonstationarity of seismicity

the SRM: (1) magnitude–frequency distribution (MFD) models; (2) distributed seismicity models (DSMs; spatial component); (3) IFMs; and (4) combining the DSM and IFM. The five sections that follow primarily provide post hoc analysis and insight, including how the SRM logic tree was reduced and comparisons with the previous NSHM (Stirling *et al.*, 2012) that are not discussed in other sections.

An important departure of the NZ NSHM 2022 from past NZ NSHMs is a focus on modeling and quantifying epistemic uncertainty; this was done for both the SRM and the GMCM components, and was an expectation of the funders of the revision. The focus on epistemic uncertainty permeates all components of the model, as outlined in Table 1.

Figures 1–3 introduce the crustal, subduction interface, and slab logic trees, respectively. The details of the logic trees are discussed throughout this article.

The NZ NSHM 2022 is a model used by both government and private industry, and a key use of the model is to underpin building code requirements. To align with a revision of these requirements, it was necessary to complete the NZ NSHM 2022 within a ~2-year time frame.

Forecast time window

There is always an inherent time component for any hazard forecast, whether that be time independent or targeting a specific time window. The determination of this time window and an occurrence rate for it must be cognizant of: (1) the limitations of the data used to construct models; (2) the forecast skill of the models for different time windows; and (3) time window implications and interests for end users. The component SRM occurrence models are constrained by three data sources: earthquake geology, geodesy, and the earthquake catalog. Leaving to the side that most of these data sources are, in fact, models themselves, the data represent (or span) different time periods from the past. Even within a specific data source, for example, earthquake geology, the time period represented within the dataset itself is often heterogenous (e.g., Fig. 4). A model and forecast based on each of these datasets, or different subsets or different interpretations of these datasets, may best represent different time windows. What these time windows are is not well known. In general, the classes of models used in the NZ NSHM 2022 are based on assumptions that result in likely realizations of the model that forecast futures that are similar to the past; however, there are many realizations possible from the models and the overall NSHM. In other words, the models extrapolate from whatever time period the data are assumed to represent to an equivalent scale future time window; however, as discussed subsequently, some exceptions are made to this to account for uncertainties around this assumption. Typically, in seismic hazard analysis, it is assumed that earthquake occurrence rates are stationary in time, and that the data represent a long-term mean of a Poisson process and, therefore, a time-independent rate can be forecast; to be specific, this refers to the true long-term mean rate whether or not the influence of aftershocks are included. In addition, it is assumed that a nominal long-term forecast will provide the most useful forecast to end users of the model. However, there is uncertainty around how well the existing data represent the long-term mean if earthquake occurrence is stationary in time, and, hence, how well a model based on this assumption can forecast the long-term hazard. There are many assumptions made when developing a time-independent forecast. First, it is assumed that there is a true and meaningful long-term mean rate; second, and perhaps more importantly, it is assumed that

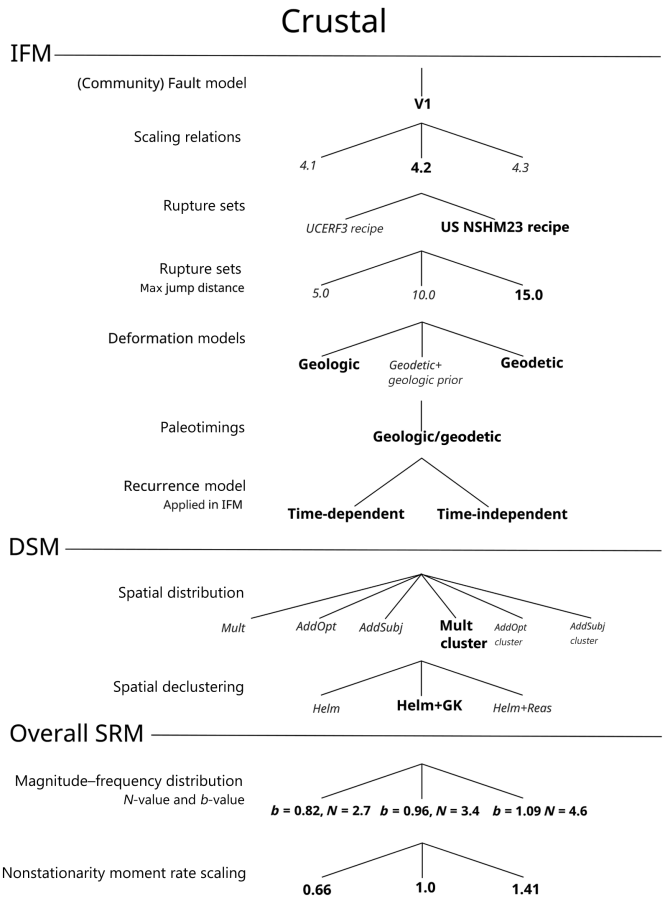

Figure 1. Crustal logic tree for the seismicity rate model (SRM). Labels in black represent the final model choices. The dark gray labels are branches that have been removed through sensitivity analyses discussed throughout this article. The branches are grouped and labeled by which component of the SRM they pertain. Branch weights are discussed in Gerstenberger, Bora, *et al.* (2022); Gerstenberger *et al.* (2024).

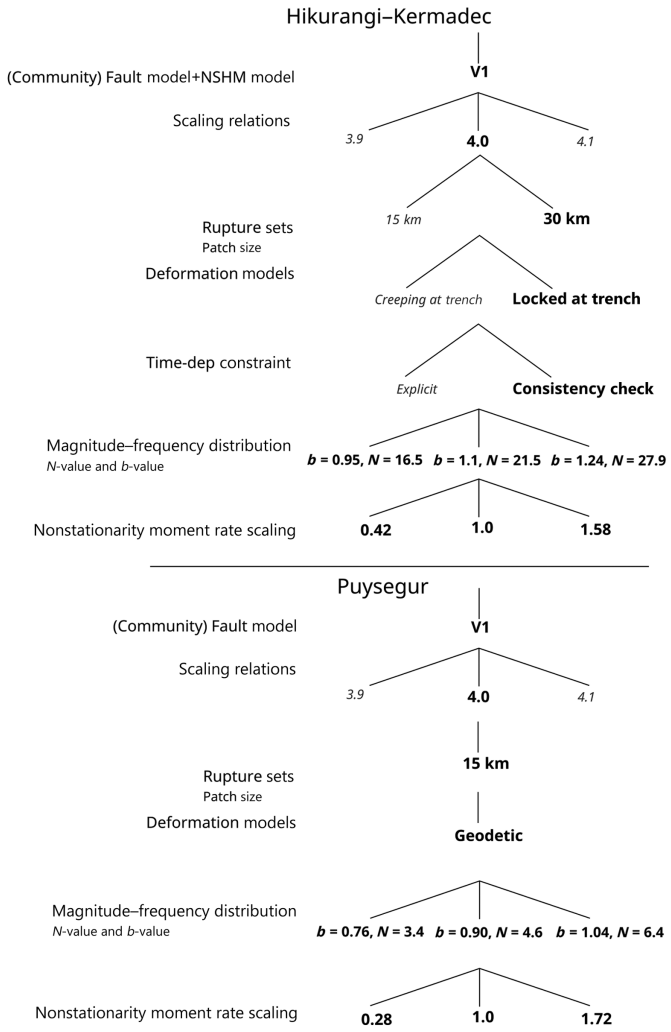

Figure 2. Subduction interface logic tree for the SRM. Labels in black represent the final model choices. The dark gray labels are branches that have been removed through sensitivity analyses discussed throughout this article. Branch weights are discussed in Gerstenberger, Bora, *et al.* (2022); Gerstenberger *et al.* (2024).

we have sufficient data and methods to estimate the long-term rate in a manner that provides skillful forecasts; third, it is often assumed that there can be robust estimates of the epistemic uncertainty in the long-term mean rate; and, finally, it is assumed that a long-term rate provides the most useful forecast to users of hazard models. Although all of these assumptions are reasonable to make, they all contain significant uncertainty and can make it easy to disregard uncertainty that is relevant to many decisions made based on hazard model results (and hence make it difficult to pass on the existence of the uncertainty and implications to users of the model). It is unknown if it is a reasonable assumption that earthquake occurrence rates are stationary in time. In other words, the complete scales of earthquake occurrence and interaction (i.e., clustering) processes are unknown. And, because they are unknown, this predetermines that there must always be uncertainty in our knowledge of: (1) if there is a true long-term mean rate; (2) what the long-term mean rate is; and (3) what length of datasets are required to make a useful estimate of the long-term rate. Lacking homogeneous and complete earthquake catalogs of lengths of thousands of years, we can only use short-term catalogs to gain insight into the variability in occurrence rate. In New Zealand, we are limited to 50–70 yr for high-quality catalogs and since ∼1840 C.E. for a lower quality catalog.

Iturrieta *et al.* (2022, 2024a) analyzed the variability in occurrence rate over the last ∼40 yr in New Zealand, Japan, California, and Italy. They demonstrate that there is large variability in the rate, for any given multidecadal-scale time period in New Zealand (Fig. 5). Japan exhibits similar behavior, whereas California and Italy show lesser dispersion in the rate. In addition, the New Zealand and Japan data exhibit nonstationarity. At the least impactful level, this variability introduces uncertainty in our ability to estimate the mean from this time period; more impactful is the potential for there to be long-term variability in the mean that is not captured, or sufficiently

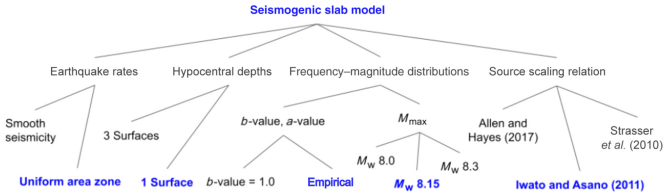

Figure 3. Slab model logic tree with final branches is shown in blue. The color version of this figure is available only in the electronic edition.

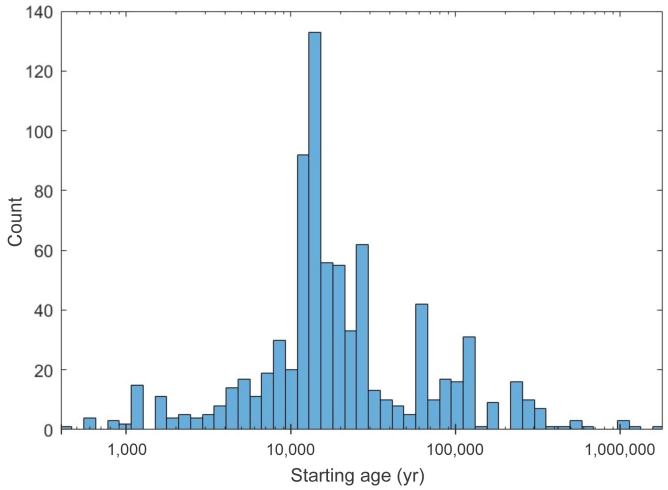

Figure 4. A histogram of the starting ages from which slip-rate estimates are determined in the New Zealand Community Fault Model version 1.0 (NZ CFM v.1.0) Seebeck *et al.* (2022, 2023). Many of the estimates cover the time span from the starting age until now; however, some are determined from observations shorter than the entire time span. This introduces variability into the data and uncertainty into our understanding of for what forecast time span the data are relevant. The color version of this figure is available only in the electronic edition.

constrained to be characterized, in any of the available datasets. This could lead to estimates of the mean that are a significant departure from the true mean. We know there are variations in the yearly and multidecadal scale, as well as variations at the thousand-year scale (e.g., fault-slip rates; e.g., Van Dissen *et al.*, 2020; Zinke *et al.*, 2021; Griffin *et al.*, 2022) and the million-year scale (i.e., plate tectonics); it is therefore not an unreasonable assumption that there may be variations in the "long-term" mean rate at scales not captured, or as yet characterized, in our existing datasets.

However, the critical point is not to determine what is the correct mean rate but to acknowledge that there is uncertainty around what this rate is and that by limiting estimates to a nominal long-term rate, we would be: (1) ignoring potentially significant epistemic uncertainty in our understanding of earthquake occurrence; and (2) not providing hazard estimates, including window-specific epistemic uncertainties, for the most useful time windows for most New Zealand decisions based on the NZ NSHM 2022. Although low probabilities of exceedance (PoE) may be used in some hazard-based decisions, there are no uses where long-term time windows are used and where long-term hazard estimates are required. NZ NSHM-based decisions are for time windows of approximately one century and for as short as one year. Therefore, the NZ NSHM 2022 forecast time window is nominally the next 100 yr and provides epistemic uncertainty specific to that time window. In this way, the model best targets the uses of the model. In addition, the modeled epistemic uncertainty can include forecasts from models developed based on different datasets and different assumptions of stationarity of seismicity rates. Ultimately, the forecasts are weighted in a logic tree framework in which a degree of belief that the forecast represents the occurrence rate for the next 100 yr is applied. It should be noted that this does not preclude a forecast from a traditional long-term model from being the most highly weighted. We also note that making a forecast for a nominal time-independent time window does not remove subjective judgment, it shifts it to assumptions about the determination of what an observed rate represents, including assumptions about what uncertainties can be usefully estimated that are relevant to end users of the model.

For NZ NSHM 2022, the goal is not to provide a hazard model that includes short-term clustering time dependence, but rather to acknowledge that there is epistemic uncertainty in our understanding of the stationarity of earthquake occurrence and to include this in the model. Although the forecast is nominally for the next 100 yr, the precision of most component models of the NSHM is not able to distinguish between, for example, 50 and 150 yr. This is particularly true of the subjective weighting of logic tree branches. However, for constraining the model and uncertainty framework, we maintain that there is a clear distinction between "the next 100 years" and "time independent" or "long term", the latter two of which often get used interchangeably.

An additional implication of this is that time dependence has also been included for the fault-based inversion models to target 100 yr. The time-dependent fault models were combined with the alternative time-independent models in the logic tree and weighted by the degree of belief that these models provide the best forecast for the next 100 yr (Christophersen and Gerstenberger, 2024).

Related, and as detailed in later sections, the overall rates of earthquakes are not declustered. The spatial component of the model can be considered declustered of short-term aftershock influence; however, the influence of active clusters (e.g., in the Canterbury and Cook Strait region) is retained. This is consistent with the recent research (e.g., Marzocchi *et al.*, 2015; Gerstenberger *et al.*, 2020; Field *et al.*, 2022) recommending the use of non-declustered overall rates for more robust hazard estimates and simplification of model calculations. This is also consistent with other recent national or large hazard models (Gerstenberger *et al.*, 2020; Kolaj *et al.*, 2020; Meletti *et al.*, 2021; Petersen *et al.*, 2023).

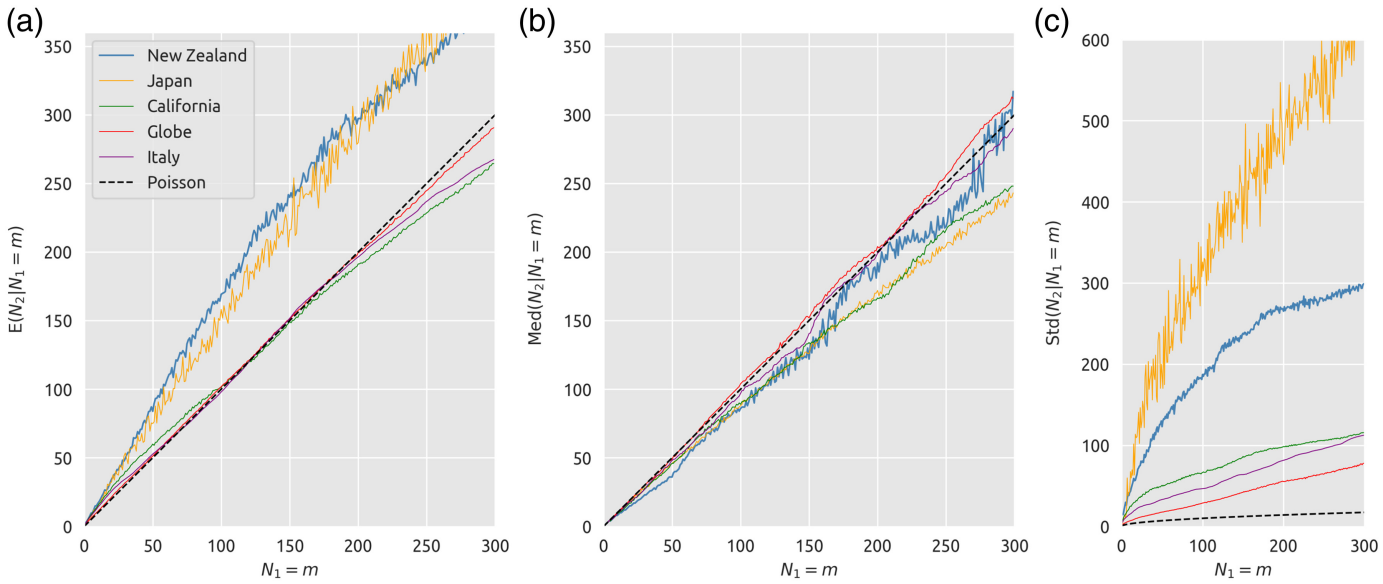

Figure 5. This figure from Iturrieta *et al.* (2024a) compares three statistics taken from sampling multiple two consecutive and equivalent length time periods (N_1 and N_2) of a catalog. The start of the N_1 time period is randomly sampled from the catalog, and m events are selected. N_2 is the consecutive period of the same length. (a) Mean; (b) median; and (c) standard deviation. Regional catalogs were filtered in time from 1980 onward, whereas the global catalog was obtained from 1991 for $M_w \geq 6$. It is observed that only the globe, Italy, and California exhibit evidence of first-order stationarity, because the mean remains constant between the training and forecasting periods, whereas New Zealand and Japan do not. The median of N_2, as opposed to the mean, tends to be closer to N_1 for all catalogs. All catalogs analyzed possess a greater dispersion than expected by Poisson behavior. See Iturrieta *et al.* (2022, 2024a) for more discussion of this figure. The color version of this figure is available only in the electronic edition.

In summary, we aim:

- for the next 100-year forecast, because it is more relevant to the time frames of decisions made using the NZ NSHM 2022 than long term; and
- to acknowledge the strengths and weaknesses of available data for constraining earthquake rates.

MODEL CONCEPT AND CONSTRUCTION

New Zealand sits astride a plate boundary, and experiences high rates of earthquakes from both crustal and subduction-related sources (Fig. 6). Here, we provide a brief overview of the SRM modeling components with more detail provided in later sections. The SRM consists of two primary components, each with multiple component models of their own: (1) the inversion-based fault model (IFM); and (2) the DSM. The IFM forecasts earthquakes only on known faults, as defined in the upper plate and subduction interface deformation models (Van Dissen *et al.*, 2022, 2024). The DSM forecasts earthquakes everywhere, and does not specifically place them on the large faults characterized in the upper plate and subduction interface deformation models; hence, the DSM does not discriminate if the earthquake is on an unknown or known fault source (Iturrieta *et al.*, 2022, 2024a; Rastin, Rhoades, Rollins, Gerstenberger, and Christophersen, 2024). The DSM (see the DSM section) consists of a hybrid seismicity model and a uniform rate zone model (URZ). The hybrid model statistically optimizes the combination of multiple components, based on different datasets, into a single forecast. The components used are the earthquake catalog-based smoothed seismicity models, geodetic strain rate, and locations of active faults and their geologic-based slip rates (Rastin *et al.*, 2022; Rastin, Rhoades, Rollins, Gerstenberger, and Christophersen, 2024). The URZ uses broad geodetic strain-rate-based zones to define areas of uniform occurrence rate (Iturrieta *et al.*, 2022, 2024a). The IFM is based on the "Grand Inversion" recipe of the Uniform California Earthquake Rupture Forecast 3 model (UCERF3; Field *et al.*, 2014). This process, for NZ NSHM 2022, is covered in detail in the IFM section. In brief, the foundation of the IFM is rupture sets generated based on possible rupture combinations of the fault sections defined in the deformation models. Earthquake occurrence rates are placed onto these ruptures using the inversion method by solving for the best solution to jointly fit the constraints provided to the inversion. The key constraints are: (1) deformation models that define the location and slip rate on each fault section; (2) the regional Gutenberg–Richter b-value; (3) the number of events of $M_w \geq 5$ (hereafter referred to as the N-value); and (4) the recurrence interval of large earthquakes where there are observations of this. The inversion method also ingests the spatial distribution of earthquakes in the DSM model to ensure that the sum of the NZ NSHM 2022 occurrence rates matches the MFD defined by the b- and N-values. As described in later sections, the NZ NSHM 2022 includes some changes to the UCERF3 recipe. These originate from

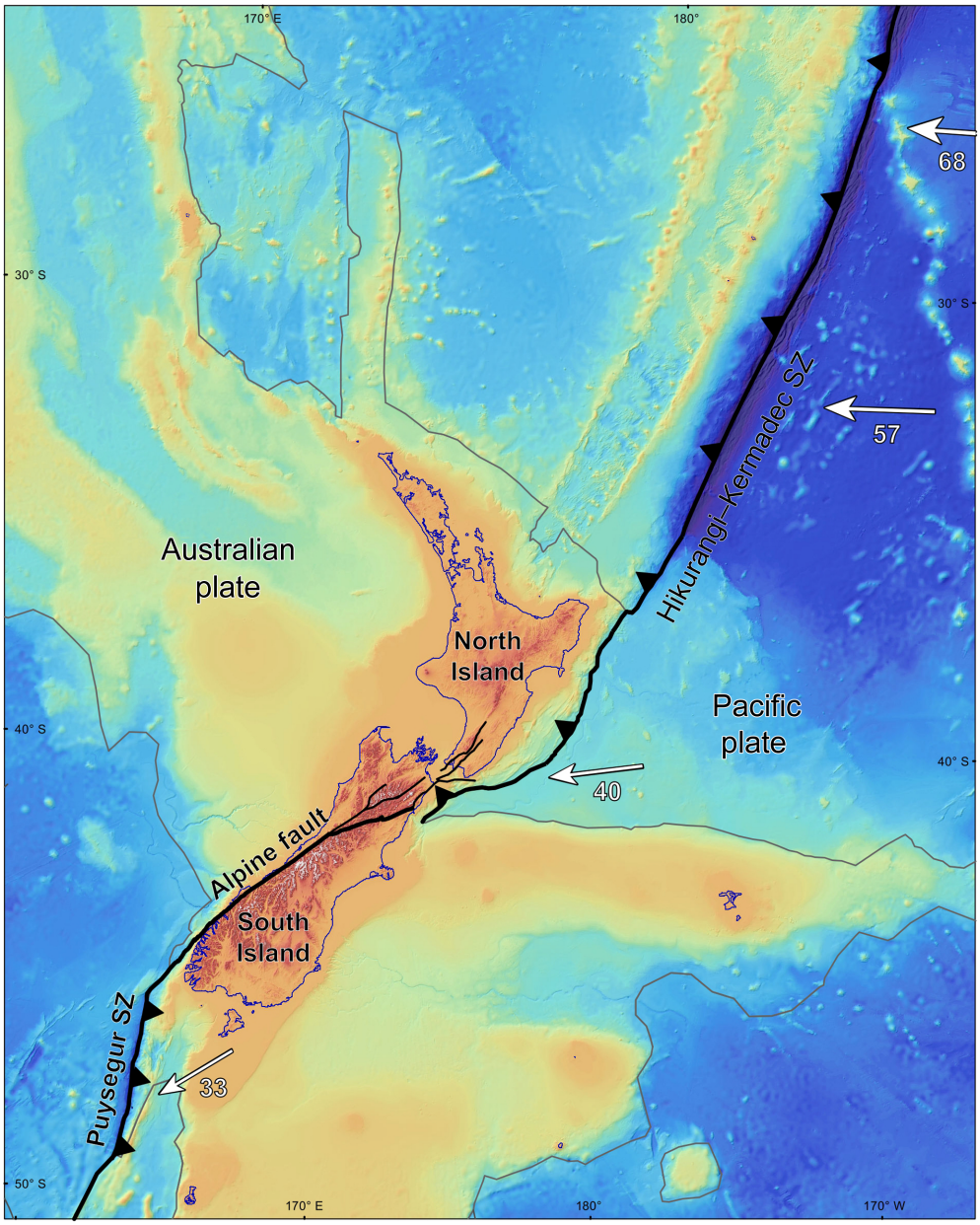

Figure 6. The New Zealand tectonic setting from Gerstenberger *et al.* (2024) and based on Mortimer *et al.* (2020). The white arrows indicate the relative Pacific plate motion with respect to the Australian plate. The black thin line denotes the transition from predominantly oceanic to predominantly continental crust. Color shading denotes elevation, which ranges from the maximum of about 4000 m above the sea level to the minimum of ∼−10,000 m below the sea level. The color version of this figure is available only in the electronic edition.

specific needs of New Zealand tectonics, differences in philosophies of the two models, and adoption of changes implemented for the forthcoming 2023 US NSHM revision due to closely working with the 2023 US NSHM team (Milner and Field, 2023; Petersen *et al.*, 2023). Table 2 lists key component models focused on those that have multiple models in which alternatives are applied in the logic tree. Outlining the details of these models, and the datasets on which they are based, is the focus of the remainder of this article. Figures 1–3 show the indicative logic trees for crustal and interface models, respectively. All combinations between the upper plate and interface models are used for the hazard calculations.

The DSM and IFM are combined for the hazard calculations via a spatial weighting in which the DSM is down weighted in grid cells near explicitly modeled faults. The DSM employed in NZ NSHM 2022 represents an important philosophical departure from other NSHMs. On its own, the DSM can be considered a complete model of earthquake occurrence that is informed by multiple datasets. The hybrid model has tested and demonstrable forecast skill at decadal time scales (e.g., Rhoades *et al.*, 2016), and hence represents a credible model for consideration in the NZ NSHM 2022; we aim to retain the influence of the DSM across all magnitudes at all locations and not consider only IFM-based rates for larger magnitudes near explicitly modeled faults. For additional context, due to a paucity of data, there is always uncertainty about how to relate any statistical optimization of a seismic hazard component model to the future. This includes catalog-based models and fault-slip-rate-based models. Catalog-based models are typically tested for: (1) shorter time periods (e.g., decades) than are the primary target of NSHMs; and (2) on predominantly moderate magnitudes (with the exception of the Every Earthquake A Precursor According to Scale (EEPAS) model, which is introduced in subsequent sections and is based on global scaling relations of large magnitudes (Rhoades and Evison, 2004, 2005). Although slip-rate data are typically a key component of hazard estimates, how to rigorously test slip-rate-based models is a challenge for which the earthquake hazard modeling community has not yet found a satisfactory answer. For these reasons, there remains uncertainty about which models are optimal models for use in seismic hazards.

TABLE 2
Key Seismicity Rate Model Component Models

Component	Rupture Sets	Deformation Models	Gutenberg–Richter *b*-Values	*N*-Value $M_w \geq 5.0$	Magnitude–Area Scaling Relation	Recurrence Intervals of Past Events	Nonfault-Based Spatial Distribution of Events
Description	Possible ruptures including multifault	Locations and slip rates for larger upper-plate faults and subduction interfaces	Shape of the MDF for the entire model	Number of earthquake $M_w \geq 5.0$	To estimate magnitude and coseismic displacement for a given fault area	Geologically determined rates of the largest events	Spatially continuous model of earthquake occurrence rate based on multiple datasets
Affects IFM or DSM	IFM	IFM	IFM and DSM	IFM and DSM	IFM	IFM	IFM and DSM
Number of models used	Single model	Single model of fault geometries and multiple models of slip rate	Multiple models	Multiple models	Multiple models	Single hybrid model	Multiple models

DSM, distributed seismicity model; IFM, inversion fault model.

More discussion related to this topic is presented in the subsequent sections.

SRM DATASET CURATION AND UNDERPINNING MODELS

All of the forecast component models of the SRM are constrained by the existing datasets, which, generally, should be considered models themselves, and which contain their assumptions. In this section, we introduce the key datasets that underpin the entire SRM model.

New Zealand Community Fault Model

The New Zealand Community Fault Model version 1.0 (NZ CFM v.1.0) was compiled, in part, for NZ NSHM 2022, and is described in detail in Seebeck *et al.* (2022, 2023). The locations and geometries of the faults explicitly modeled in NZ NSHM 2022 are taken directly from the NZ CFM v.1.0. In addition, the geologic-based fault-slip rates utilized in the geologic deformation model come directly from the NZ CFM v.1.0, as do the geologic prior slip rates used in a component of the geodetic deformation model. In brief, the NZ CFM v.1.0 is an object-oriented, simplified 2D and 3D representation of active fault zones in New Zealand and adjacent offshore regions (including a selection of potentially seismogenic faults) compiled at a nominal scale of 1:500,000–1:1,000,000. Within the model, crustal fault zones have a constant dip with depth, whereas the two subduction interfaces (Hikurangi and Puysegur) have variable dips with depth. Through community engagement, the NZ CFM v.1.0 updates the active fault model of New Zealand (Litchfield *et al.*, 2014) and extends the updated fault zones from the surface to seismogenic depths using seismicity and thermal modeling constraints (Ellis *et al.*, 2022, 2024). NZ CFM v.1.0 fault zones are defined based on surface geology, seismicity, seismic reflection profiles, wells, and geologic cross-sections. The model presently comprises 880 fault zones and fault zone sections in two complementary datasets. The first dataset is a 2D map representation of active (or potentially active) fault zone traces with associated geometric and kinematic attributes such as dip and dip direction, maximum seismogenic rupture depth, sense of movement, rake, and net slip rate. This 2D representation of the NZ CFM v.1.0, with faults projected to depth according to dip, is the fault representation used in NZ NSHM 2022. The second dataset is a 3D-triangulated representation of the fault surfaces. Because of fault zone intersections and linkages in the 3D representation of the model, there are important differences between the 2D and 3D representations users should be aware of. Full details of these differences can be found in Seebeck *et al.* (2022, 2023). NZ CFM v.1.0 is at present a single, expert-led, explicit model representation of active and potentially seismogenic fault zones. With the exception of the Puysegur subduction interface, version 1.0 does not yet incorporate alternative interpretations of fault geometry.

Earthquake geology database

The New Zealand Paleoseismic Site Database version 1.0 (Litchfield *et al.*, 2022, 2024) contains earthquake geology (paleoseismology) data collected at specific sites along active faults throughout New Zealand. These data are grouped into three primary categories/datasets: (1) slip rate; (2) earthquake timings and recurrence interval (RI); and (3) single-event displacements (SEDs). The paleoseismic site database was developed as part of the NZ NSHM 2022 with its primary purpose being to compile paleoseismic data at specific sites to be used either as inputs into or to constrain/validate outputs from the IFM component of NZ NSHM 2022. For example, the earthquake timings and SED data compiled in the paleoseismic site database are used directly to determine fault recurrence intervals that are employed as constraints in the IFM (e.g., Coffey *et al.*, 2022, 2024). The earthquake timings data, in particular, the timing of the most recent event/rupture, are also used to

incorporate conditional probability of rupture into aspects of the IFM. In addition, the slip-rate data compiled in the paleoseismic site database was used in the parameterization of fault-slip rates in the NZ CFM v.1.0.

The New Zealand Paleoseismic Site Database version 1.0 contains both published and unpublished data, mostly onshore, at a total of 2136 sites with a reasonable geographic spread of across New Zealand, particularly along onshore faults with slip rates of ≥1 mm/yr. The slip rate dataset contains 862 sites situated on 183 different NZ CFM v.1.0 fault sections. The earthquake timings dataset encompasses 304 sites and 953 records (single-site and combined-site records) on 99 different NZ CFM v.1.0 fault sections. This dataset contains over 280 sites with the most recent event timing records, 97 sites with timing records for three or more earthquakes, and 98 previously reported recurrence interval records. The SED dataset contains 970 sites situated on 90 different NZ CFM fault sections. The majority of SED sites are field-based displacement measurements for historical earthquakes dominated by the 2010 Darfield and 2016 Kaikōura earthquakes.

Geodetic strain rate

To incorporate geodetic measurements of contemporary deformation into NZ NSHM 2022, strain rate and fault-slip deficit rate models are developed utilizing New Zealand's interseismic Global Navigation Satellite Systems (GNSS)-derived velocity field (Johnson *et al.*, 2022, 2024; Maurer *et al.*, 2024).

Derivation of the strain-rate models starts with the published Global Positioning System-derived velocity field of Beavan *et al.* (2016). This velocity field is based on the data acquired between 1995 and 2013, and includes corrections for the recent earthquakes during that period such as the 2010/2011 Canterbury earthquake sequence and, therefore, represents interseismic deformation spanning 1995–2013. Because the goal of developing the strain-rate models is to use them to solve for slip deficit rates on crustal faults, deformation signals that are evidently not the result of interseismic locking on crustal faults, such as suspected sill cooling in the Taupō volcanic zone (TVZ) and coupling on the Hikurangi subduction interface, have been removed from the velocity field (Johnson *et al.*, 2022, 2024).

From the amended velocity field, strain-rate maps are computed using two purely statistical methods and two elasticity-based methods (Johnson *et al.*, 2022, 2024; Maurer *et al.*, 2024). The statistical methods include VELMAP, which solves for a spatially smooth velocity field by balancing the misfit between fitting observed velocities and minimizing the Laplacian of the velocity field (Wang and Wright, 2012; Weiss *et al.*, 2020). The other uses geostatistical methods of variogram analysis and kriging to build realizations of the velocity and strain-rate fields with covariance structure inherent to the observed velocities. The physics-based methods derive a continuous velocity field using elasticity solutions. These methods solve for a distribution of body forces in an elastic thin plate that explains the observed velocity field and then compute the strain-rate field from the estimated distribution of forces. The vertical derivatives of horizontal stress (VDoHS) method uses the finite-element method to compute elastic responses (Haines *et al.*, 2015; Haines and Wallace, 2020), whereas the body force method uses analytical Green's functions (Sandwell and Wessel, 2016) and damped least squares to solve for the strength of the forces (Johnson *et al.*, 2024).

The principal result from the strain-rate maps derived from the four different methods is that the mean maximum shear strain rate is similar across all methods (Fig. 7), whereas the spatial distribution of dilatation and strain-rate style differs more significantly. The maximum shear strain rate averaged across the country varies between about 0.1 and 0.12 microstrain/yr (~20% variation), and the dilatation rate between about 0.015 and 0.023 microstrain/yr (~40% variation).

Magnitude–area scaling relations

Every fault rupture in the rupture sets is ascribed a magnitude using magnitude–area scaling relations. In the literature, there are numerous such scaling relations (see Shaw, 2013; Stirling *et al.*, 2013, 2021, 2024; Shaw *et al.*, 2022), for more details. For NZ NSHM 2022, we developed a "backbone" magnitude–area scaling relation (Stirling *et al.*, 2021, 2024) that encompasses the salient features and spread of the most applicable relations for both crustal and subduction interface ruptures (Stirling *et al.*, 2013, 2021; Shaw *et al.*, 2022; Stirling *et al.*, 2024). The resulting "backbone" relation has the functional form of: $M_w = \log_{10} A + C$, in which A is the rupture area in km^2; and the C values for crustal and interface ruptures are as follows:

- C values for crustal ruptures: 4.1, 4.2, and 4.3; and
- C values for subduction interface ruptures: 3.9, 4.0, and 4.1.

Every rupture in the rupture sets of NZ NSHM 2022 is also ascribed an average coseismic displacement based on the above "backbone" magnitude–area scaling relation and specific values of C. This is done through the application of the Hanks and Kanamori (1979) seismic moment (M_0)—moment magnitude relation of: $M_0 = 10^{1.5M_w+9.05}$, and then solving for average coseismic displacement (D) using the Aki (1966) relation of $D = M_0/(Ax\mu)$ and crustal rigidity $\mu = 3.0 \times 10^{10}$ N · m^2.

3.5 Standardized magnitude earthquake catalog

Use of the GeoNet earthquake catalog magnitudes directly for hazard calculations proves challenging for at least three different reasons: (1) earthquakes occurring prior to 1900 have significant uncertainties in magnitude and location; (2) the local magnitude scale (M_L) varies through time; and (3) limited moment magnitudes (M_w) are available, and these are required for correlating the SRM with the GMCM.

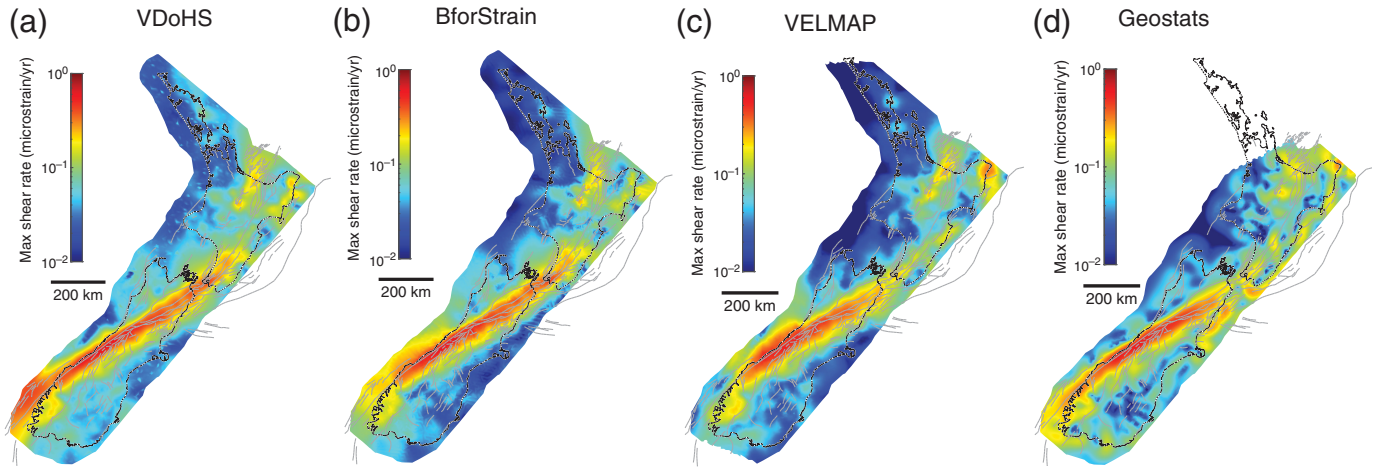

Figure 7. The four geodetic maximum shear estimates. (a) Vertical derivatives of horizontal stress (VDoHS); (b) BforStrain; (c) VELMAP; and (d) Geostats. The color version of this figure is available only in the electronic edition.

Around 30 GeoNet M_w between 1848 and 1993 have magnitudes inconsistent with the published studies. For these, we adapted the magnitudes from the published work, which changed the magnitudes of the affected earthquake by around 0.1 magnitude units in most cases (Rollins *et al.*, 2021; Rollins, Christophersen, *et al.*, 2024).

To address the second point, magnitude revisions undertaken for NZ NSHM 2022 corrected for changes in the M_L scale since 1931 and standardized these M_L magnitudes to match to M_w when a true M_w was not available (Christophersen *et al.*, 2022, 2024). The two local magnitudes in the GeoNet earthquake catalog are: (1) MLNZ77 for between 1931 and 2012, which uses NZ-specific attenuation relations (Haines, 1981a,b); and (2) MLSC3 from 2012 onward, which follows the original local magnitude definition for California (Richter, 1935). A new magnitude, MLNZ20, was derived from the vertical amplitude readings of Wood–Anderson synthetic waveforms and with attenuation relations to, on average, match M_w (Rhoades *et al.*, 2020). MLNZ20 was calculated for all earthquakes with sufficient digital waveform recordings, covering the time from the early 2000s until 2020. Applying a careful data selection regression relations were derived for MLNZ20 on MLNZ77 and on MLSC3 so that a proxy could be calculated when only MLNZ77 or MLSC3 was available in the dataset. This way a proxy for M_w could be derived from local magnitudes going back to 1931. Two additional steps were done for larger earthquakes. MLNZ77 (>5.55) was converted to M_w based on (Rhoades and Christophersen, 2017). In addition, an additional regression was developed for M_w versus MLSC3 for M_w >4.55. This was used for earthquakes post-2012 that had no M_w estimate. The combined result is a catalog of standardized magnitudes, M_{std}, that, on average, are consistent with those back to 1931. (Christophersen *et al.*, 2022, 2024). Noticeably, this reduces the rates of M_w >5 by about half when compared to using the currently preferred GeoNet magnitude.

MFD MODELS AND MOMENT-RATE VARIABILITY

Two critical constraints in the SRM are the overall number of earthquakes forecast of $M_w \geq 5$ (N-value) and the magnitude distribution that they follow (b-value): jointly we call these constraints the MFD constraint (Rollins *et al.*, 2022; Rollins, Gerstenberger, *et al.*, 2024). The NZ NSHM 2022 approaches this differently than the previous NZ NSHMs in that these parameters are considered to be forecast parameters that we can constrain rather than them being an output of the NSHM based on other decisions within the model. The two primary components of the SRM (i.e., the DSM and the IFM) are influenced at different levels by the MFD constraint. For the DSM, the forecast DSM will be exactly as constrained by the MFD; for the IFM, there is a trade-off between the different parameters used to constrain the IFM (see IFM discussion subsequently). This results in the influence of the MFD being less powerful over the IFM occurrence rate than it is for the DSM. One caveat is that in the magnitude range that overlaps between the two component models (M_w 6.9–8.0), the DSM rates are reduced by the IFM rates using the method described in the Combining the DSM and IFM section subsequently. The MFD constraints are broken down into four regions: (1) crustal; (2) Hikurangi–Kermadec subduction interface; (3) Puysegur subduction interface; and (4) slab (i.e., seismicity in the downgoing plate below the subduction interface for both the Hikurangi–Kermadec and Puysegur subduction zones). A single MFD is provided for each region that is constrained by the NZ NSHM 2022 earthquake catalog described earlier. For the Hikurangi–Kermadec interface, the catalog is supplemented with additional global data, as described in Rollins *et al.* (2021); Rollins, Christophersen, *et al.* (2024).

Despite the revisions done for the NZ NSHM 2022, the earthquake catalog still presents many challenges related to quality and consistency, which increase the uncertainty in the MFD constraint. Three specific challenges are: (1) a poor understanding of the magnitude of completeness and the significant impact this has on any estimates; (2) a significant bump in the MFD for

TABLE 3
***N*-Values and *N*-Scaling**

Model Component	Time Period	Mean *b*- and *N*-Value Pairs	N-Scaling Factor
Crustal	1951 – 2020[a]	$b = 0.96$, $N = 3.4$/yr[b]	$2\sigma^a = (0.59,1.41)$
	1843 – 2020[b]	$b = 0.82$, $N = 3.9$/yr[b]	$2\sigma^b = (0.74,1.40)$
		$b = 1.09$, $N = 6.4$/yr[a]	
IFM	1951 – 2020[a]	$b = 0.96$, $N = 3.4$/yr[b]	$2\sigma^a = (0.59,1.41)$
	1843 – 2020[b]	$b = 0.82$, $N = 2.7$/yr[b]	$2\sigma^b = (0.74,1.40)$
		$b = 1.09$, $N = 4.6$/yr[b]	
		$b = 1.10$, $N = 21.54$/yr	
Hikurangi–Kermadec subduction	1965–2019	$b = 0.95$, $N = 16.54$/yr	Global $2\sigma = (0.42,1.58)$
		$b = 1.25$, $N = 27.9$/yr	
		$b = 0.90$, $N = 4.6$/yr	
Puysegur subduction zone	2000–2019	$b = 0.76$, $N = 3.4$	Moment-scaled $2\sigma = (0.28,1.72)$
		$b = 1.04$, $N = 6.4$/yr	

Superscripts indicate which method and result are paired. For crustal and inversion fault model (IFM) the alternative *N*-scaling factors were averaged for the final hazard calculations (0.66, 1.41).

magnitudes below 5 that is likely related to magnitude conversions; and (3) a relatively short period of better quality data (1951+ C.E.).

Surprisingly, there is significant uncertainty in our ability to estimate how many earthquakes of $M_w \geq 5$ have occurred in New Zealand when using time periods that allow for robust statistics (Rollins *et al.*, 2022; Rollins, Gerstenberger, *et al.*, 2024). Because of this, the challenges in assessing completeness and the difficulty in getting a robust Gutenberg–Richter *b*-value, it is necessary to model multiple *b*-values for the final hazard calculations. Because of the dependency of the *N*-value on the *b*-value used for each region, we couple a *b*-value estimate with its related *N*-value and hence do not sweep through all possible combinations that would produce nonsensical results. The aim for estimating the *N*-values and the uncertainty in our understanding of them was twofold. First, we wished to understand the uncertainty in estimating the mean (i.e., the standard error in the mean annual rate, not the Poisson variability), which is specific to the time period for which we have data. Second, we estimated how much the variability within a nominal 100-year time period was overdispersed when compared with a Poisson distribution (Rollins *et al.*, 2022; Rollins, Gerstenberger, *et al.*, 2024; Rastin, Rhoades, Rollins, and Gerstenberger, 2024). For the hazard logic tree, we separate the error in the mean from the overdispersion. As discussed previously, all estimates will be subjectively assessed for their applicability to the next 100 yr. All *N*-value calculations are done using a nondeclustered catalog.

Crustal MFD models

Crustal parameters are estimated for the Collaboratory for the Study of Earthquake Predictability (Gerstenberger and Rhoades, 2010) region, which includes the top 40 km and extends 50 km offshore. For crustal-related parameters, we require two sets of values (Table 3). One is for the crustal IFM, and the other is for the DSM; this is because, within the crustal zone, the DSM does not distinguish between crustal, interface, and slab earthquakes, and we need to constrain the crustal rates for the IFM. This resulted in a reduction in *N*-value for the IFM parameters but did not impact the *b*-values. The *N*-scaling factor is the scaling factor applied to the mean *N*-value to model the observed overdispersion in variability compared with the dispersion that is estimated by Poisson. Two alternative *N*-scaling (also referred to as moment-rate scaling) models are considered, and the models differ in the length of catalog used (1951–2020 and 1840–2020) and treatment of magnitude uncertainty (Rollins *et al.*, 2022; Rollins, Gerstenberger, *et al.*, 2024) and (Rastin, Rhoades, Rollins, and Gerstenberger, 2024). The difference between the models represents the trade-off between using only higher quality data of a shorter time span and including lower quality data and allowing for a longer time span. For the final hazard calculations, the average of the two models was used with lower and upper values of 0.66 and 1.41, respectively.

Interface MFD models

The interface *b*- and *N*-value pairs (Table 3) were estimated using a modified version of the NZ NSHM 2022 catalog supplemented with Hikurangi–Kermadec seismicity from International Seismological Centre-Global Earthquake Model (ISC-GEM) version 9 (Di Giacomo *et al.*, 2018), as described in (Rollins *et al.*, 2022; Rollins, Christophersen, *et al.*, 2024). The *N*-scaling for Puysegur is informed by credible ranges of coupling coefficients (0.4–1.0). The global *N*-scaling factor is calculated by modeling the overdispersion of earthquake rates, compared with Poisson, which is seen when investigating similar subduction regions around the globe (Rollins *et al.*, 2022; Rollins, Gerstenberger, *et al.*, 2024). For Puysegur, the regional *N*-scaling parameters are considered too narrow, as discussed subsequently, and we therefore do not propose to use these values in the final hazard calculations.

Intraslab MFD models

Based on the uncertainty analysis presented in (Thingbaijam, Gerstenberger, *et al.*, 2022; Thingbaijam *et al.*, 2024), we do not consider uncertainty in the MFD parameters in the subduction zone slabs. The *b*- and *N*-value pairs are listed in Table 4. *N*-scaling parameters were not calculated for the subduction slabs, and that is left for the future revision of the NSHM.

Correction to interface *N*-scaling from moment-rate variability

We consider the interface estimates of both the *N* and the *N*-scaling to be poorly constrained for the Hikurangi portion of the Hikurangi–Kermadec interface and also for the Puysegur interface due to a paucity of data. To better understand this, we

TABLE 4
N-Values for Slab

Hikurangi–Kermadec Mean *b*- and *N*-Value	Puysegur Mean *b*- and *N*-Value
$b = 1.06$, $N = 5.91$	$b = 1.15$, $N = 0.64$

directly compared the range of moment estimates from the crustal *N*-scaling to those of the interface. Because of the greater uncertainty in nearly all aspects of the interface modeling, we consider that the range of moment rate considered for the interface model should not be less than for the crustal model. Without *N*-scaling, the total crustal IFM moment release range that is considered based on the model parameters ranges from 1.08×10^{19} N · m to 2.72×10^{19} N · m. When the crustal *N*-scaling is applied to this moment-rate range, it results in a dispersion (±2 sigma) of 6.02 across the moment-rate distribution.

Without *N*-scaling, the total moment range considered for the Hikurangi–Kermadec interface is 7.43×10^{19} N · m to 2.28×10^{20} N · m. When the global *N*-scaling is applied (Table 3) to this total moment range, it results in a dispersion of 13.0. This is twice the total moment range considered in the crustal IFM. The larger moment range considered by the Hikurangi–Kermadec interface is considered justified by the large uncertainties in the coupling of the interface (Van Dissen *et al.*, 2022, 2024), and in the *b*-value and *N*-value parameters.

For the Puysegur interface, we use a single inversion model for computational and weighting reasons; so there is no epistemic uncertainty in the Puysegur IFM. To introduce a sufficient epistemic uncertainty, we scale the single IFM to a sufficiently wide moment-rate range via *N*-scaling. We believe that the moment-rate range we consider for Puysegur should not be as large as that for Hikurangi–Kermadec, due to the smaller size and smaller maximum magnitude of the Puysegur interface. However, we think the Puysegur moment-rate range should not be less than that for the crustal IFM, due to the large uncertainties in the coupling coefficient and the rates of moderate and large earthquakes (Van Dissen *et al.*, 2022, 2024; Rollins, Gerstenberger, *et al.*, 2024). For this reason, we scale the Puysegur *N*-scaling values by a factor of 6.02, which produces a moment range dispersion that is equivalent to the dispersion considered for the crustal IFM. We enforce that the low-end and high-end *N*-scaling values should be symmetric about 1. Together with the range of 6.02 between them, this uniquely constrains the *N*-scaling to be [0.28, 1.72].

DSMs (SPATIAL COMPONENT)

For the NZ NSHM 2022, the DSM has been separated into spatial and rate components. In other words, we have developed a spatial distribution over which different total forecast rates (*N*-value) can be distributed. The rate component is discussed in the MFD Model section. The DSM spatial component has four components that have been developed individually:

- shallow (<40 km depth) hybrid model;
- crustal URZ model;
- interface model ($M_w < 7.5$); and
- slab model.

For the final hazard implementation, the crustal hybrid model (from now on referred to as the "hybrid model") and the crustal URZ are combined as described later in this section. The specific details are explained subsequently, but we have separated declustering into two components for the final DSM: (1) overall rate; and (2) spatial distribution. The overall rate is not declustered when some spatial declustering is applied.

Crustal hybrid model

The hybrid model brings together multiple datasets and models to produce a spatially gridded forecast for $5.0 \le M_w \le 8.0$ for all of New Zealand (Rastin *et al.*, 2022; Rastin, Rhoades, Rollins, Gerstenberger, and Christophersen, 2024) and for earthquakes shallower than 40 km depth. The hybrid model is defined on a grid with 0.1° spacing. Multiple forecasts have been developed and optimized based on the revised New Zealand earthquake catalog (Rollins *et al.*, 2021; Rollins, Christophersen, *et al.*, 2024; Christophersen *et al.*, 2022, 2024) using data from 1951 to 2020 when the catalog is complete for $M_w > 4.95$. The hybrid model does not distinguish among crustal, interface, or slab events.

A set of catalog-independent and smoothed seismicity covariates are constructed using a variety of datasets and component models, and used in the final hybrid candidate models (Rastin *et al.*, 2022; Rastin, Rhoades, Rollins, Gerstenberger, and Christophersen, 2024). These covariates are:

- SUP—baseline spatially uniform Poisson model: A uniform rate model that is scaled by the other hybrid component models;
- PPI—proximity to plate interface: Based on the depth-averaged reciprocal of the shortest distance from points in a cell to a point on the plate boundary, represented by either the Hikurangi subduction interface, the Hope fault, the Alpine fault, or the Puysegur subduction interface;
- PMF—proximity to mapped faults including slip rate: Based on the depth-averaged reciprocal of distances from points in a cell to points on faults, weighted by the slip rate of the fault in the geologic deformation model;
- HWS—geodetic shear strain rate: The geodetic shear strain estimated at all locations using the VDoHS method of Haines and Wallace (2020) and as used as a contributor to the geodetic deformation model of the NZ NSHM 2022 (Johnson *et al.*, 2022, 2024);
- FLT—fault location: A zero or one binary value based on whether or not a cell in the DSM is intersected by an active fault in the NZ CFM v.1.0 (Seebeck *et al.*, 2023);
- PPE—Proximity to the past earthquakes smoothed seismicity model: An isotropic smoothed seismicity model with a power law kernel (Rhoades and Evison, 2004);

- G50—a Gaussian 50 km kernel smoothed seismicity model: Based on Frankel (1995) and as implemented in the previous NZ NSHMs (Stirling *et al.*, 2002, 2012); and
- Helm—a density-based smoothed seismicity model: An adaptive Gaussian kernel method (Helmstetter and Werner, 2012; Rastin, Rhoades, Rollins, Gerstenberger, and Christophersen, 2024) in which the smoothing distance is determined based on the density of earthquake observations.

To create the multiplicative hybrid model, the SUP model was scaled by the covariates using an optimized multiplier for each. Such multiplicative hybrids have been shown to provide significantly better forecasts than any of the individual components (Rastin *et al.*, 2022; Rastin, Rhoades, Rollins, Gerstenberger, and Christophersen, 2024) and the references therein when tested over 70 yr of catalog with results primarily controlled by moderate magnitudes. Rastin *et al.* (2022) also developed additive hybrid candidate models as alternative options for regions where multiplicative modeling further attenuates existing low values of covariates intrinsically; however, these models were not used and are not discussed here.

A benefit of DSMs is that they generally can be statistically tested and optimized against existing earthquake catalog data. Notwithstanding limitations due to the dominance of moderate-magnitude earthquakes and high-seismicity regions in testing results, such testing and optimizations can still provide a quantitative basis to inform model building. Fitting and subsequent model selection are based on the likelihood-based Information Gain Per Earthquake (IGPE) statistic (Rhoades, Schorlemmer, *et al.*, 2011).

In New Zealand, the earthquake catalog from 1951 to the present is sufficiently complete at small enough magnitudes ($M_w > 4.95$) for constraining the hybrid model. These 70 yr of data can be considered to be independent of the data used in PPI, PMF, and HWS; however, they are not independent of the data used to create the smoothed seismicity forecasts. To handle this, the models have been optimized using seven different fitting periods of equal length. For example, in the first fitting period, the component models were derived from the earthquake catalog from 1961 to 2020. The fitted component models were then used as an input for fitting the hybrid model to the target earthquakes from 1951 to 1960. This was repeated for seven different fitting periods, and the average of the seven time-constrained smoothed seismicity covariates forms the smoothed seismicity covariate. The hybrid model parameters were optimized using the IGPE criterion, based on all earthquakes from all the seven periods but with different smoothed seismicity catalog inputs in each period. The average hybrid model forecast across all the seven periods was used to determine the final hybrid model forecast. Although individual components had been based on declustered catalogs, the hybrid model optimization was based on a full (nondeclustered) catalog. This was done because: (1) if we fit a declustered catalog, we are biasing toward the chosen decustering method; (2) we aimed to be as objective as possible in the fitting; (3) there is essentially no difference across methods when average models are created; and (4) the IGPE is insignificantly different between fitting a declustered and nondeclustered catalog. Finally, the use of a hybrid model minimizes the chance of biasing toward existing aftershock sequences when compared with traditional smoothed seismicity models.

Four different declustering methods have been tested as part of the hybrid model development. Helm applies its declustering method based on the median rate in each cell over 20-day time windows; within the time constraints of this project, we were not able to change that or explore alternative implementations, and the Helm declustering method was retained for this model. For the remainder of the smoothed seismicity models, we explored the impact of using the following methods: (1) Gardner and Knopoff (1974); (2) Grünthal (1985), a modification to Gardner and Knopoff; and (3) Reasenberg (1985). The declustering parameters are discussed in Rastin *et al.* (2022); Rastin, Rhoades, Rollins, Gerstenberger, and Christophersen (2024).

Ultimately the impact of the declustering method was shown to insignificantly impact the forecasting skill of the hybrid model (Rastin *et al.*, 2022; Rastin, Rhoades, Rollins, Gerstenberger, and Christophersen, 2024). In addition, the different methods lead to only small differences in the spatial forecasts. The insensitivity of the IGPE to the particular declustering method is due to: (1) the influence of the overall number of events being removed by testing only on the spatial component; and (2) the use of multiple covariates rather than just a simple smoothed seismicity model, which is more sensitive to the choice of declustering method. Based on these results, the NZ NSHM 2022 does not include epistemic uncertainty related to declustering. It should be noted that all declustering methods significantly reduce the influence of the ongoing Canterbury Earthquake Sequence. This is discussed in the next section.

All the possible combinations of component models were fitted in the optimization. A small range of model combinations provided the highest IGPE values; the forecast skill of these models is statistically indistinguishable (Table 5). From these best models, the final model was chosen based on the following criteria:

- hybrids containing the most informative components, that is, those with the highest IGPE when combined with SUP individually; and
- hybrids with the highest or near to the highest IGPE.

The most informative smoothed seismicity covariate overall is Helm. The most informative nonsmoothed seismicity covariate is PMF followed by HWS. Overall, the best-performing hybrid model is a multiplicative combination of SUP, PMF, HWS covariates and an average of the three smoothed seismicity models; this is the hybrid model used in the NZ NSHM 2022.

TABLE 5
Information Gain Per Earthquake (IGPE) for Best-Performing Hybrid Models, All Use the Average of a Gaussian 50 km Kernel Smoothed Seismicity Model (G50), Proximity to Past Earthquakes (PPE), and a Density-Based Smoothed Seismicity Model (HELM)

Declustering (for G50 and PPE)	Full Hybrid Model	SUP, Smoothed Seismicity, PMF, and HWS	SUP, Smoothed Seismicity
GRU	0.84	0.85	0.74
GK74	0.83	0.84	0.74
RES	0.83	0.84	0.74
None	0.72	0.73	0.62

In all cases HELM uses its own internal declustering method. HWS, geodetic shear strain rate; PMF, proximity to mapped faults including slip rate; and SUP, baseline spatially uniform Poisson model.

Adding in medium-term clustering

The NZ NSHM 2022 aims to provide an estimate of earthquake hazards for about the next 100 yr. To supplement the hybrid model for this timeframe, the medium-term forecasting model EEPAS (Evison and Rhoades, 2004; Rhoades and Evison, 2004; Rhoades and Christophersen, 2019; Rastin *et al.*, 2021) can provide additional forecasts specific to the earthquakes expected to occur over the next decade or two. Often, it gives information gains that are higher than those of the hybrid models discussed in the previous sections. This suggests that hybrid DSMs can be improved by mixing them in appropriate proportions with EEPAS model forecasts for the next decade or two.

The fundamentals of the EEPAS models are scaling relations between a regional cumulative magnitude, time, area, and mainshock magnitude (Evison and Rhoades, 2004; Rastin *et al.*, 2021). Regional cumulative magnitude is defined as: for each forecast target earthquake, the magnitudes of all the previous earthquakes are precursory magnitudes; however, for a target earthquake, only the smaller and nearby earthquakes make considerable contributions to the forecast. The EEPAS model does not inherently forecast a complete Gutenberg–Richter distribution.

To include time-varying information on expected earthquake spatial distribution over the next few decades, the EEPAS model must be combined with the hybrid model for implementation in the NZ NSHM 2022. This is done by applying a 20% weighting to the EEPAS spatial contribution and an 80% weighting to the hybrid model. Ultimately, this is subjective but is chosen to reflect the 20-year timeframe over which the EEPAS contribution is most significant over the 100-year forecast window of the NZ NSHM 2022. Although using an average of four EEPAS versions should improve robustness, the NZ NSHM 2022 does not include uncertainty related to this averaging, other effects of parameter uncertainties in the EEPAS component, or the combination with the hybrid model. These are left to the future NSHMs.

The final crustal hybrid model

Six models from Rastin *et al.* (2022) were considered in hazard sensitivity tests (Gerstenberger, Van Dissen, *et al.*, 2022; Rastin, Rhoades, Rollins, Gerstenberger, and Christophersen, 2024). In hazard sensitivity testing, using hazard maps and selected hazard curves, the difference within the classes of models including EEPAS and those not including EEPAS-based models was very small when compared with other uncertainties in the NZ NSHM 2022. In addition, it was not considered defensible to use a model that considers the Canterbury Earthquake Sequence to be over and forecasts earthquakes in Canterbury at rates prior to 2009 due to the continued increased activity in the Canterbury region (Gerstenberger, Van Dissen, *et al.*, 2022). In addition, we did not use the alternative additive hybrid model options, which, subjectively may better address low-seismicity regions than a multiplicative hybrid model, because the URZ covers for the regions with the lowest seismicity and acts as a floor for the spatial distribution (see the URZ forecast model and flooring the hybrid model section). Finally, based on the sensitivity testing for the NZ NSHM 2022, the only model used is the "Multiplicative Total" that averages the three smoothed seismicity models and is integrated with EEPAS model. The spatial distributions at M_w 6.0 are shown in Figure 8.

Hikurangi–Kermadec and Puysegur subduction interface DSMs

As discussed in the IFM section subsequently, the IFM only models rates of interface earthquakes for $M_w \geq 7.5$. Earthquakes of $5.0 \leq M_w < 7.5$ are modeled within the DSM. The model uses a $0.1° \times 0.1°$ grid that is distributed on the same interface geometry as used for the IFM, with one caveat; for optimization of calculation speed, the entire Hikurangi–Kermadec interface was not considered, and the northern end of the Hikurangi–Kermadec DSM is terminated at roughly −37° latitude. Earthquakes of $M_w < 7.5$ do not provide a significant contribution to hazard at distances farther offshore. Only a single layer of grids is used. The spatial distribution is derived from the geodetic-based slip deficit rate, as developed for the interface deformation model (see the Deformation models for a discussion of the deformation model development). For consistency with the IFM, the "locked to trench" slip deficit rate model was chosen. For this distribution, the slip deficit rate model was normalized to a total value of 1.0. Earthquake or fault-strike orientations were constrained to be trench parallel to be consistent with the IFM.

The Puysegur subduction interface does not have a specific DSM. Earthquakes of $M_w < 7.0$ are modeled in the hybrid model. Within the extent of the Puysegur interface, 56% of the rate is assigned to interface events (Rollins *et al.*, 2022). Earthquakes of $M_w \geq 7.0$ are modeled in the IFM.

Depth distribution model for the DSM

The depth distribution of events in the DSM is based on the revised catalog of (Rollins *et al.*, 2021; Rollins, Christophersen,

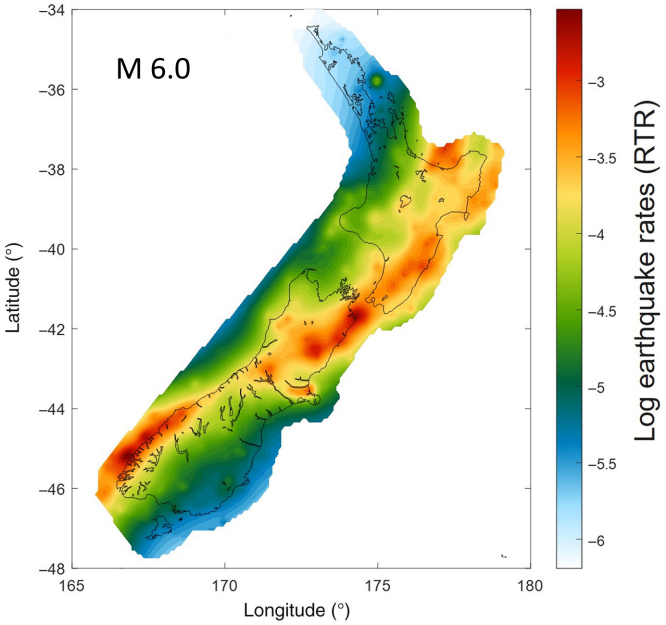

Figure 8. Shown is the spatial distribution at M_w 6.0 of the final hybrid "Multiplicative Total" model, which averages the three smoothed seismicity models and is integrated with the **E**very **E**arthquake A **P**recursor **A**ccording to **S**cale (EEPAS) model. Log earthquake rates are shown relative to a reference model (RTR units) in which one earthquake per year is expected to exceed any magnitude m in 10 m per km^2. Because the EEPAS model is not constrained to be Gutenberg–Richter, there can be very subtle spatial differences across magnitude bins; however, M_w 6, as shown in this figure, is representative of the full magnitude range. The color version of this figure is available only in the electronic edition.

et al., 2024), including the probabilistic tectonic zonation in depth. To account for regional variations in depth distributions, four different regional depth distributions have been applied: (1) crustal; (2) crustal above the Hikurangi interface; (3) crustal above the Puysegur interface; and (4) TVZ. In addition, some intraslab events are assigned to depths shallower than 40 km (Rollins *et al.*, 2021; Rollins, Christophersen, *et al.*, 2024) and are handled in the slab model (Thingbaijam, Gerstenberger, *et al.*, 2022).

Three different depth discretizations of the top 40 km have been explored for their impact on hazards. Comparisons of national-scale hazard maps and hazard curves across six different hybrid models for four cities were done. No significant differences were seen across 3, 4, or 5 layers. Three layers were used for optimization of hazard calculations.

Earthquake mechanisms and fault-plane orientations for the crustal DSM

A probabilistic characterization of the focal mechanisms (or a focal mechanism model) were used to define the predominant styles and orientations of virtual fault ruptures for $M_w > 6.5$ events in the NZ NSHM2022 crustal DSM (Thingbaijam, Rattenbury, *et al.*, 2022; Thingbaijam *et al.*, 2023). The focal mechanism model was developed using a range of datasets that include: (1) the neotectonic domains and faulting styles (orientations and rakes) defined in the NZ CFM v.1.0 (Seebeck *et al.*, 2022, 2023); (2) the domain-specific assessment of fault-strike orientations (Edbrooke *et al.*, 2014; Rattenbury, 2022); and (3) the GeoNet regional moment tensor catalog (Ristau, 2013).

In each neotectonic domain, the distribution of the strike angles, represented by mean and standard deviations, is adapted from that given by Rattenbury (2022), whereas predominant dip angle and rake angles are defined based on the evaluation of the NZ CFM v.1.0. To account for different faulting styles, another distribution for the rake angles is incorporated, which differs from the first one, particularly, in two regions; first, much of the South Island (excluding the Otago region and the southeast Zealandia platform) where strike-slip mechanisms are assigned, and, second, the Hikurangi margin region, where normal faulting mechanisms are assigned to account for observed normal faulting events within the subducting Pacific plate. Thus, we have two cases for the spatial distribution of the rake angles: the first one is given by NZ CFM v.1.0; and the second one is based on the published literature and expert judgments. These two cases are considered aleatoric and given equal weights to define a single model for the focal mechanism. In the final NZ NSHM 2022 implementation, an optimal representation consisting of only mean estimates of strike angle and mode estimates of other parameters but for both the cases of rake variability has been used, following a hazard sensitivity analysis.

URZ and non-Poisson hazard

An important shortcoming of the hybrid models is that their forecast skill is unknown in low-seismicity regions. In addition, since the hybrid fitting and optimization are based on locations where earthquakes have occurred since 1951, there is little information included to constrain rates in low-seismicity regions. This suggests that the rates and epistemic uncertainty in low-seismicity regions are poorly constrained by the range of hybrid models considered. For this reason, we applied URZs (Iturrieta *et al.*, 2022, 2024a), which are based on large zones of uniform earthquake occurrence rate. These large zones acknowledge that our ability to constrain the spatial distribution of rates within these low-seismicity zones is poor. Another aspect of the uncertainty in low-seismicity regions that we address with the URZs is the variability in rate. Typically, in seismic hazard evaluations, this variability is assumed to be Poisson (Gerstenberger *et al.*, 2020). Iturrieta *et al.* (2022, 2024a) show that the variability in the future rate increases beyond what Poisson variability predicts as the number of observed events available to constrain the future rate of events decreases.

Iturrieta *et al.* (2022, 2024a) aimed to constrain this uncertainty by looking at the rate variability that occurs across consecutive equivalent length time periods (i.e., observation and forecast) when the number of earthquakes is small. The analysis was performed for New Zealand, Japan, California, Italy, and the entire globe. Regional catalogs of $M_w \geq 4.0$ were used

and fit from 1980 to 2020; the global catalog was fit from 1991 for $M_w \geq 6.0$. This analysis shows, for Japan and New Zealand, that the distribution of occurrence rates is skewed, and that the forecast mean rate is more likely to be higher than the observed rate of events (Fig. 5); in other words, the occurrence rates of events are clustered (overdispersed) from, for example, aftershock, and there is also evidence of nonstationarity (the mean is not constant in time; (Iturrieta *et al.*, 2022, 2024a). These conditions may indicate that a Poisson distribution with a mean rate sampled from low event counts underpredicts the mean rate in a forecast time horizon. Interestingly, this skewness is not observed for California and Italy.

Iturrieta *et al.* (2022, 2024a) also tested, using IGPE, the ability of a simple smoothed seismicity model (Gaussian 50 km smoothing) to forecast the spatial distribution of rates better than the least-informative spatially uniform model, particularly, when the numbers of observed earthquakes are small. For both New Zealand and Japan, they show that when there are roughly fewer than 200 events in a region, the smoothed seismicity model was less skillful than the spatially uniform model.

The zones for the model were developed independently of seismicity data and relied on the geodetic strain-rate field of Haines and Wallace (2020). Multiple methods were examined to discretize the strain-rate field into three or more zones. The final implementation uses three zones determined using the principle of minimum description length (Fayyad and Irani, 1993; Ramírez-Gallego *et al.*, 2016), which is a user-independent method that allows compression of the data minimizing the loss of information. Sensitivity testing showed that the final hazard was not sensitive to the number of discretizations or methods used.

URZ forecast model and flooring the hybrid model

By its nature, the design of URZs in the NZ NSHM 2022 has defined zones for high- and low-seismicity regions. However, the goal of the URZs was to better forecast seismicity in lower seismicity regions, and the URZ was only applied as the minimum rate floor within the lowest strain-rate zone. This zone crosses the plate boundary and for application, the zone in the north of New Zealand is treated independently from the zone from Canterbury to Stewart Island.

Negative binomial hazard calculations

To capture the occurrence rate variability, a temporal model based on the negative binomial distribution has been implemented into the OpenQuake (Pagani *et al.*, 2014) engine (Iturrieta *et al.*, 2024b). This model can replace the standard Poisson calculations used in probabilistic seismic hazard analysis (PSHA). It requires a mean forecast rate and a dispersion parameter Iturrieta *et al.* (2022, 2024b). The dispersion parameter was determined based on empirical analysis of the datasets from New Zealand, Italy, Japan, and California (e.g., Fig. 5) and as described in Iturrieta *et al.* (2022, 2024b). Importantly, this calculation also changes the standard PSHA procedure, which considers only the probability of one or more earthquakes. The negative binomial implementation integrates over the probability of one or more, two or more, three or more, and so forth, earthquakes. These approaches are equivalent to normal Poisson calculations. However, when using non-Poisson temporal models for high rates of exceedance, the difference can become noticeable. Moreover, in the NZ NSHM 2022, we only apply the negative binomial model in the low-seismicity-rate regions.

Intraslab seismicity models for the Hikurangi and the Puysegur subduction zones

Thingbaijam, Gerstenberger, *et al.* (2022); Thingbaijam *et al.* (2024) developed both smooth and uniform area zone seismicity models for intraslab earthquakes in the Hikurangi and Puysegur subduction zones. These models are based on the geospatial configuration of the subduction zone geometry (Van Dissen *et al.*, 2022, 2024), an updated earthquake catalog (Rollins *et al.*, 2021; Rollins, Christophersen, *et al.*, 2024), and a regional moment tensor solution catalog (Ristau, 2013) to evaluate the orientation of finite-fault ruptures (strike subparallel to trench and dips >60°). The maximum magnitude for intraslab earthquake is assumed to range between M_w 8.0 and 8.3, based on the historical, largest intraslab earthquakes across the globe, and a maximum magnitude of 8.15 was chosen. In NZ NSHM 2022, a uniform area zone seismicity model was used in the final hazard calculations.

Both interface geometries were extrapolated to greater depths (~250 km for Hikurangi and ~150 km for Puysegur) through a radial basis function that applies a linear kernel to generate smooth surfaces and were truncated at ~300 km from, respectively, the northernmost and southernmost coastlines; this means slab events of the Kermadec portion are not modeled beyond 300 km distance. The resulting interface geometries are used to assign intraslab events from the earthquake catalog, and to approximate the seismicity-defined mid-slab geometry onto which the intraslab seismicity is projected and uniformly distributed.

From the updated earthquake catalog for New Zealand (Rollins *et al.*, 2021; Rollins, Christophersen, *et al.*, 2024), a subcatalog of intraslab earthquakes is extracted following the strategy developed by Pagani *et al.* (2021), as detailed in Thingbaijam, Gerstenberger, *et al.* (2022, 2024).

To define a seismic "mid-slab" surface for the two subduction slabs, 3D orthogonal distances from hypocenters (for events with $M_w \geq 3.0$) to the interface–slab boundaries were computed. For Hikurangi, the seismic mid-slab is ~28.7 km below the interface. Based on the median absolute deviation, which is equal to 12.15 km, a discrete probability distribution for the depth of the events is defined as follows: 16.5, 28.7, and 40.8 km with probabilities estimated to be 0.40, 0.40, and 0.20, respectively. For Puysegur, the seismic mid-slab is ~14.7 km below the interface. The estimated median absolute deviation

equal to 5.0 km yields the minimal depth probability distribution with depths at 9.7, 14.7, and 19.7 km with probabilities equal to 0.32, 0.40, and 0.28, respectively.

To inform logic tree branch selection for the subduction zone intraslab models, Thingbaijam, Gerstenberger, *et al.* (2022); Thingbaijam *et al.* (2024) undertook a suite of hazard sensitivity studies across a range of branch choices, including, type of seismicity model (uniform or smooth), number of seismicity depth surfaces (one or three), *b*- and *a*-values, M_{max}, and scaling relations. The various branch choices did not have a significant impact on resulting hazard (typically less than 10%), and single branch options were chosen in NZ NSHM 2022 for each of the considered choices, as indicated in Figure 3. In addition, the evidence in support of *b*-value = 1 was poor, and it was not considered necessary to include it as a credible alternative to the assessed *b*-value with the large numbers of events (1655 $M_w \geq 4$ for Hikurangi, 228 $M_w \geq 4$ for Puysegur) used to estimate *b*-value.

IFM

For the IFM, we have based our procedure on the UCERF3 earthquake rupture forecast building recipe (Field *et al.*, 2014), but with some changes. The basic concept with this recipe is that we develop thousands of potential fault-rupture scenarios, and, then, we invert for the rate of each of the potential rupture scenarios using various model and data-based constraints. The rate for any particular (potential) rupture in the final solution is allowed to be zero. The procedure is that we have: (1) a collection of potential ruptures; (2) an MFD that applies to the region that contains the ruptures; (3) a slip rate for all faults within the fault network; and (4) a geologically determined recurrence interval for a specified magnitude range for a small subset of locations within the fault network: From these we determine the earthquake occurrence rates that best satisfy all the constraints. This large and underdetermined matrix inversion problem is solved using the UCERF3 simulated annealing method, as described in (Page *et al.*, 2014). We have used the OpenSHA implementation of the 2023 US NSHM team (Milner and Field, 2023) for the inversion set up and solution calculations. We have revised the UCERF3 recipe, including revisions from (Milner *et al.*, 2022; Milner and Field, 2023), as discussed in the following sections. The key steps in developing the IFM are described in the following sections, but can be summarized as follows:

1. Fault model: Defines the geometries of the upper plate and subduction interface active fault earthquake sources. This starts with the NZ CFM v.1.0 for the upper-plate faults, and this relies on compilations based on the previously published literature for the subduction interfaces.
2. Subsections: Create subsections for each active fault earthquake source. For crustal faults, each subsection has a length, nominally, one-half of the down-dip width of the fault. For the subduction interfaces, these are tiled into 15 km × 15 km patches (Puysegur) or 30 km × 30 km patches (Hikurangi–Kermadec).
3. Rupture sets: Construct the rupture set by connecting together subsections into plausible ruptures. Our plausibility filters for upper-plate faults include; (1) the maximum jump distance ≤15 km; (2) cumulative of the absolute values of slip-rake change of ≤360°; (3) the minimum number of subsections of two; and (4) a range of Coulomb stress thresholds (see Milner *et al.*, 2013, 2022). Our plausibility filters for subduction interfaces are much simpler and revolve around limiting the aspect ratios of ruptures such that the length-to-width rupture aspect ratio is constrained to lie within the range of 1:1–5:1 until the full width of the interface source is reached, and then rupture length can grow unlimited; an additional filter is that a rupture patch on the interface (30×30 km^2 for the Hikurangi–Kermadec and 15×15 km^2 for the Puysegur) can only rupture once in a specific rupture event.
4. Magnitude–area scaling relations: Determine the magnitude and average coseismic displacement of each rupture.
5. Deformation models: Estimate the slip rate for every subsection based on either geologic or geodetic considerations (or a combination of both).
6. Recurrence times: Estimate recurrence times for large events ($>M_w$ 6.9) on all crustal fault subsections with sufficient earthquake geology data.
7. *N*-value (number of events): Estimate the mean rate of events of $M_w \geq 5$ in the earthquake catalog.
8. *b*-value: Estimate the Gutenberg–Richter *b*-value from the earthquake catalog.
9. Spatial rate distribution: Derive the spatial distribution of earthquakes from the DSM.
10. Fault polygons: Create 3D polygons around all crustal faults in the fault model (e.g., using a 12 km distance from the fault trace). Fault polygons were not applied to the subduction interfaces.
11. Rate partitioning: For upper-plate fault, split the *N*-value contribution into on-fault and off-fault components based on the percentage of the spatial probability density function that is inside and outside of the fault polygons.
12. Target MFD: Determine the target MFD for the inversion based on the on-fault *N*-value and *b*-value for ruptures above an assumed minimum magnitude (IFM M_{min}).
13. Inversion: Run the inversion to determine the set of occurrence rates on individual ruptures that optimally satisfy the constraints.
14. Recurrence times smoothing constraint: Within each fault section that contains a subsection with a recurrence time constraint, apply an occurrence rate smoothing constraint to minimize strong rate variations along strike. This was only applied to upper plate faults.

IFM overview and assumptions

The aim, and power, of the IFM is to find multiple known-fault-based earthquake occurrence rate solutions that satisfy the constraints from across different datasets and models. In the previous two NZ NSHMs (Stirling *et al.*, 2002, 2012), the occurrence of large earthquakes was essentially controlled by a single geological estimate of slip rate per fault section (and a single scaling-relation-based estimate of coseismic slip) leading to a single estimate of both recurrence interval and earthquake magnitude. In addition, Stirling *et al.* (2012) included a limited number of multifault ruptures, but including complex ruptures of many faults was challenging. Two of the primary motivations for using the inversion method were to better address these challenges by: (1) allowing for the use of multiple occurrence rate constraints; and (2) including a comprehensive suite of multifault ruptures, including high-impact low-probability earthquakes that rupture many faults (>10), extend for 100s of kilometers and occur infrequently (e.g., >20 ky). Toward these goals, in the IFM, and the SRM, in general, we added two classes of uncertainty. The first is uncertainty in the occurrence rates of events, as informed by different datasets, and the second is the uncertainty in the earthquake geology and geodetic slip rates, the earthquake timings data, and magnitude–area scaling relations. Both the classes of uncertainty contain both epistemic uncertainty and aleatory variability, and are modeled as such. We consider that models built using our three main datasets can each provide credible forecasts of the future earthquakes. As discussed in the Forecast time window, exactly what future time window these models relate to is uncertain. For the inversion method slip rates and paleoearthquake timings exert the most significant influence on the rates of large events. The target MFD and, hence, the earthquake catalog do influence the rate of large events, but to a lesser degree than the other datasets. Because of the uncertainty around what forecast time windows the earthquake geology, geodesy, and earthquake catalog-based models represent, the forecast time window of an inversion-based forecast is not precisely known. The NZ NSHM 2022 target forecast time window of 100 yr provides a framework to subjectively assess the skill (or degree of belief) of each of the forecast for that time window. We note that the true forecast time window is never precisely known in any seismic hazard model; it is always assumed.

Tectonics and regionalization

The calculation of the IFM has been separated into three zones based on tectonic types. We independently calculate occurrence rates for crustal faults, the Hikurangi–Kermadec subduction zone interface, and the Puysegur subduction zone interface. Different from past NZ NSHMs, we do not regionalize crustal *b*-values; due to the uncertainties in the magnitudes, the challenges in assessing the completeness magnitude and the low number of data points, a regional b-value was not justified (Rollins *et al.*, 2022, Rollins, Gerstenberger, *et al.*, 2024). A limitation of separating the crustal model from the interface models is that joint ruptures of the interface with crustal faults are not considered. Based on the 2016 M_w 7.8 Kaikōura earthquake and the 1855 M_w 8.2–8.3 Wairarapa earthquake, it is quite likely that joint crustal–interface ruptures do occur. Allowing joint ruptures introduces enormous complexity in terms of: (1) constraining the nearly infinite possible combination of ruptures; (2) understanding the scaling of slip; and (3) modeling of ground motions. Constraints on these are currently scarce. Solving uncertainties associated with this complexity is left to future iterations of the NZ NSHM and is likely to be informed by historical earthquakes, simulated earthquake catalogs, and ground motions.

The second feature of the regionalization is that we have not separated the Hikurangi portion of the subduction interface from the Kermadec portion of the interface (Rollins *et al.*, 2022; Rollins, Gerstenberger, *et al.*, 2024). Modeling them separately does not allow for modeling of great earthquakes involving both subduction zones and suffers from poor constraints on *N*-value specific to the Hikurangi subduction zone; however, the inversion MFD target is dominated by the extremely productive Kermadec region by modeling them together. This potential limitation is constrained in the inversion by the strong regional variation in slip rate (slip deficit rate), which appropriately constrains the solutions to place the higher rates of events in the high occurrence rate region of the Kermadec.

IFM minimum and maximum magnitude and rate correction factor

For the crustal IFM, we have nominally constrained the minimum modeled magnitude to M_w 6.9. The most impactful constraints on the rates of large events are the deformation models and the paleoearthquake timings. In New Zealand, outside of the Taupō rift–Havre trough region, the likelihood of an $<M_w$ 6.9 event rupturing the ground surface is relatively low, and the probability of missing such events in the paleoearthquake record is high, and, therefore, the ability of the inversion method to constrain the rates of these events was considered weak, and the rates of earthquakes of $M_w < 6.9$ are modeled solely in the DSM. In rare cases, magnitudes of less than 6.9 are modeled in the IFM. This is largely an artifact of the fault model that includes a few very short faults. A slip-rate reduction of 0.1 is applied (i.e., only 90% of the slip rate is used) to the crustal deformation models outside of the Taupō rift–Havre trough region and 0.3 within the Taupō rift–Havre trough region to account for: (1) fault displacement not related to primary coseismic displacement on that fault (e.g., postseismic slip and triggered slip); and (2) the moment from earthquakes of $<M_w$ 6.9 that are not included in the IFM. For consistency, the upper-plate geodetic deformation model solutions were calculated using the same minimum magnitude and corrections factor.

Faults in the Taupō rift–Havre trough region with slip rates <1.8 mm/yr are not considered for the IFM. The complexity the large number of small faults in this region would add

considerably to the complexity of the inversion, and the large uncertainty about the geometry and connectivity of the faults at depth indicate that the complex network of smaller faults is better modeled in the DSM, where faults and their slip rates are included as part of the PMF model in the hybrid model. Maximum magnitude (M_{max}) for the crustal IFM is not an input constraint. The maximum considered magnitude is limited based on the maximum area of ruptures in the rupture set and by the particular scaling relation applied. The M_{max} in the IFM is determined by what is necessary to satisfy the constraints and may be less than the maximum magnitude represented by the largest rupture in the rupture sets; therefore, a range of M_{max} is implicitly considered in the final hazard calculations. For the subduction interface IFMs, the M_{min} is strictly a function of fault subsection size. Initially both the interface models were modeled using 15 km × 15 km square subsections. The sheer number of patches this produced for the Hikurangi–Kermadec interface was impractical for calculations, and the subsections were increased to 30 km × 30 km for the Hikurangi–Kermadec. In both the interface deformation models, the minimum rupture considered is a single subsection. For the Hikurangi–Kermadec, the minimum magnitude considered in the IFM is M_w 7.5, and it is M_w 7.0 for Puysegur. Smaller events are modeled in the DSM. Similar to the crustal IFM, a correction factor of 5% was applied to account for $M_w < 7.5$, which were not modeled in the Hikurangi–Kermadec IFM but are assumed to contribute to the slip budget. This factor is the percent of moment coming from earthquakes of $M_w <$ 7.5 with $b = 1.1$ and an M_{max} of 9.5. Also similar to the crustal IFM, the M_{max} in the interface IFM is not an input constraint and is a function of the maximum rupture area, scaling relation, and the necessary ruptures to satisfy the inversion constraints. This results in a range of M_{max} considered in the final hazard calculations. The M_{max} is about M_w 9.5 on average for the Hikurangi–Kermadec and up to M_w 8.8 is considered in the Puysegur model.

We note that Gerstenberger, Van Dissen, *et al.* (2022) incorrectly reported the use of an M_{min} of 6.8, and the correct value as implemented is M_w 6.9. As shown in the supplemental material available to this article, there are negligible differences between the use of M_w 6.8 and 6.9.

Regional MFD target

One of the critical constraints in the inversion is the target MFD, and a MFD specific to the faults and ruptures modeled in the inversion was determined. The input constraints to the model include a regional (e.g., crustal or Hikurangi–Kermadec interface) *b*-value and regional *N*-value. For the inversion constraint, the IFM-specific target was constructed from the *N*-value, *b*-value, spatial rate distribution, and fault polygons. The IFM-specific MFD was determined by the fraction of rate that fell within the polygons (Gerstenberger, Van Dissen, *et al.*, 2022).

Determining the inversion solution

The resulting inversion problem for the crustal IMF has 411,270 model unknowns (i.e., rupture occurrence rate); the Hikurangi–Kermadec and Puysegur subduction interface inversions are smaller with 23,675 and 15,800 model unknowns, respectively. This large, underdetermined inversion problem was solved using the simulated annealing method described by Page *et al.* (2014) with some modifications. Although the inversions start with a large number of possible ruptures, the final solution only requires a small subset of them to have nonzero rates to satisfy the constraints. Multiple models were run, each using a different set of parameter values; each set of parameter values resulted in a different number of nonzero ruptures to converge. The crustal inversions required between ~600 to more than 1700 ruptures and the Hikurangi–Kermadec and Puysegur inversions require a similar range.

Simulated annealing and constraint weights

To perform a simultaneous inversion that optimizes multiple constraint types (e.g., MFD, fault-slip rate, and paleoearthquake recurrence rate), weights must be chosen for each constraint to combine them into a single objective function. The individual constraint energy (sum of squared misfits) is multiplied by its respective weight before summing all constraint energies to form the total objective function to be minimized. The relative size of the chosen weights will influence the constraint that is better fit in the event they are not entirely compatible (i.e., a single solution cannot satisfy all constraints simultaneously). The determination of constraint weights is handled differently for the crustal IFM than it is for the interface IFM (Gerstenberger, Van Dissen, *et al.*, 2022). Ultimately, the weights used are a choice of the modeling team and hence should be considered an epistemic uncertainty. For the interface IFM, we have adopted the UCERF3 scheme of applying subjective weights determined by the NSHM team. For the crustal IFM, we have applied a new scheme, described subsequently and in Milner *et al.* (2022) and Milner and Field (2023), which allows for an objective determination of the weights that aims for uniformly fitting the constraints in a manner that is weighted by the uncertainty in the constraints. We have not applied this method for the interface IFM, because we do not have robust estimates of uncertainty on each deformation model. For the subduction interface, we compared multiple inversion solutions using varying weights and chose weights that were subjectively thought to provide the best balance of the constraint fits and that provided a consistent quality of fit over different inversion runs with different constraint choices (e.g., using different deformation models). We used both a normalized slip-rate constraint and an unnormalized slip-rate constraint. The normalized slip-rate constraint depends on the rate misfit (solution minus target) divided by the target slip rate, so that large misfits relative to a given slip rate are penalized. The unnormalized slip-rate constraint depends on the rate misfit so that large absolute differences are penalized.

The choice of weight was not a significant source of uncertainty when compared with other epistemic uncertainties in the NSHM; therefore, a single set of constraint weights was used in the final solutions for the interface IFM.

For the crustal inversions, we used a dynamic reweighting scheme (Milner and Field, 2023). The scheme attempts to fit all data constraints equally, relative to their uncertainties, and, therefore, only a single slip-rate constraint is necessary (with the normalization done by the uncertainty on each slip rate). It does so by calculating the misfit for each constraint in units of data standard deviation after each averaging round and adjusts the constraint weight such that the new weight = previous weight $\times\sqrt{\text{constraint misfit/average misfit}}$. In this way, the constraints that are more poorly fit get additional weight so that the inversion prioritizes improving them over other constraints. Ultimately, all constraints are fit equally well relative to their uncertainty.

The algorithm used is the Fast simulated annealing of Szu and Hartley (1987) using a perturbation function that is a random, uniformly distributed order of magnitude between 10^{-10} and 10^{-2}, which is then scaled by a uniformly distributed number between −0.5 and 0.5. This simulated annealing method was chosen, because it provided fast and reliable convergence.

Two modifications were made to the traditional serial simulated annealing algorithm to improve solution quality and speed. Thread selection was used to speed up the inversion, and thread averaging was used to reduce the chance that the inversion will become stuck in a local minimum of the objective function.

In thread selection, the simulated annealing process is performed in parallel on four simultaneous threads. The best solution from the four threads is selected every second (approximately every 400,000 iterations) and used as the starting point to continue the simulated annealing process. Four simultaneous inversions were run and averaged every 30 s (approximately every 12 million iterations).

Determining logic tree weights from inversion fits

It is inevitable that some combinations of inversion constraints are not completely compatible. For example, assumptions about the MFD function and the magnitude–area scaling relationship can result in fault-slip rates that are too slow to satisfy the slip-rate constraint. In that case, a solution may be a compromise among constraints and not reflect well any of the constraints.

When establishing weights for the SRM logic tree (not to be confused with inversion constraint weights), we included the inversion goodness of fit as an additional weighting factor to be applied in addition to the parameter weights from expert elicitation (Gerstenberger, Bora, *et al.*, 2022). In this way, we decreased the weight of parameter combinations that are not compatible and may, therefore, be less plausible.

Deformation models

As part of the NZ NSHM 2022, deformation models were constructed for the upper-plate (crustal) faults and subduction interfaces that impact ground-shaking hazard in the country (Johnson *et al.*, 2022, 2024; Van Dissen *et al.*, 2022, 2024). Following the UCERF3 workflow (Field *et al.*, 2014), these deformation models provide the locations, geometries, and slip rates of the earthquake-producing faults explicitly modeled within the NZ NSHM 2022. For the upper-plate faults, two deformation models were developed: one using geologic-based slip rates and the other using geodetic strain-rate-based slip deficit rates (Fig. 9). For the two subduction interfaces proximal to New Zealand, two deformation models are developed for the Hikurangi–Kermadec interface, which lies to the east and northeast of the North Island, and a single model for the Puysegur interface, which lies to the southwest of the South Island (Fig. 6).

Development of the upper-plate geologic deformation model (Fig. 9a) is described in Van Dissen *et al.* (2022, 2024) and, with only slight amendment, is derived directly from the fault geometries and slip rates characterized in the NZ CFM v.1.0 (Seebeck *et al.*, 2022, 2023). The upper-plate geodetic deformation model (Fig. 9b) utilizes the same fault geometry model as the geologic model but with fault-slip deficit rates derived by inverting geodetic strain rate (Johnson *et al.*, 2022, 2024). The geodetically derived strain rates were developed using four different methods (VDoHS, body-force method, VELMAP, and geostatistical), as described in Johnson *et al.* (2022, 2024) and Maurer *et al.* (2024), based on the published interseismic GNSS-derived velocity field of Beavan *et al.* (2016).

The geometry and slip deficit rates for the Hikurangi–Kermadec subduction interface deformation model are blends of a variety of data, constraints, and interpretations of Van Dissen *et al.* (2022, 2024). The geometry of the Hikurangi–Kermadec deformation model is a linear blend of the Hikurangi interface geometry of Williams *et al.* (2013) and the Slab 2.0 Kermadec interface geometry of (Hayes *et al.*, 2018). Derivation of slip deficit rates on the Hikurangi portion of the deformation model are founded on the well-established block modeling methods described in Wallace *et al.* (2004, 2012) with "locked to trench" and "creeping at trench" slip deficit rate renditions defined. The details of these derivations are presented in Van Dissen *et al.* (2022, 2024). Slip deficit rate for the Kermadec portion of the Hikurangi–Kermadec subduction interface deformation model is based on convergence rate (Power *et al.*, 2012) and locking (coupling coefficient) considerations. The two Hikurangi slip deficit rate renditions ("locked to trench" and "creeping at trench") are smoothly combined with the single Kermadec slip deficit portrayal to yield two alternative slip deficit rate characterizations for the Hikurangi–Kermadec interface (Van Dissen *et al.*, 2022, 2024). The two Hikurangi–Kermadec deformation models were initially developed to explore epistemic uncertainty in ground-shaking hazard that may be a consequence of the two different slip deficit rate renditions. However, based on hazard sensitivity evaluations undertaken as part of the NZ NSHM 2022, it was found that there was no difference in

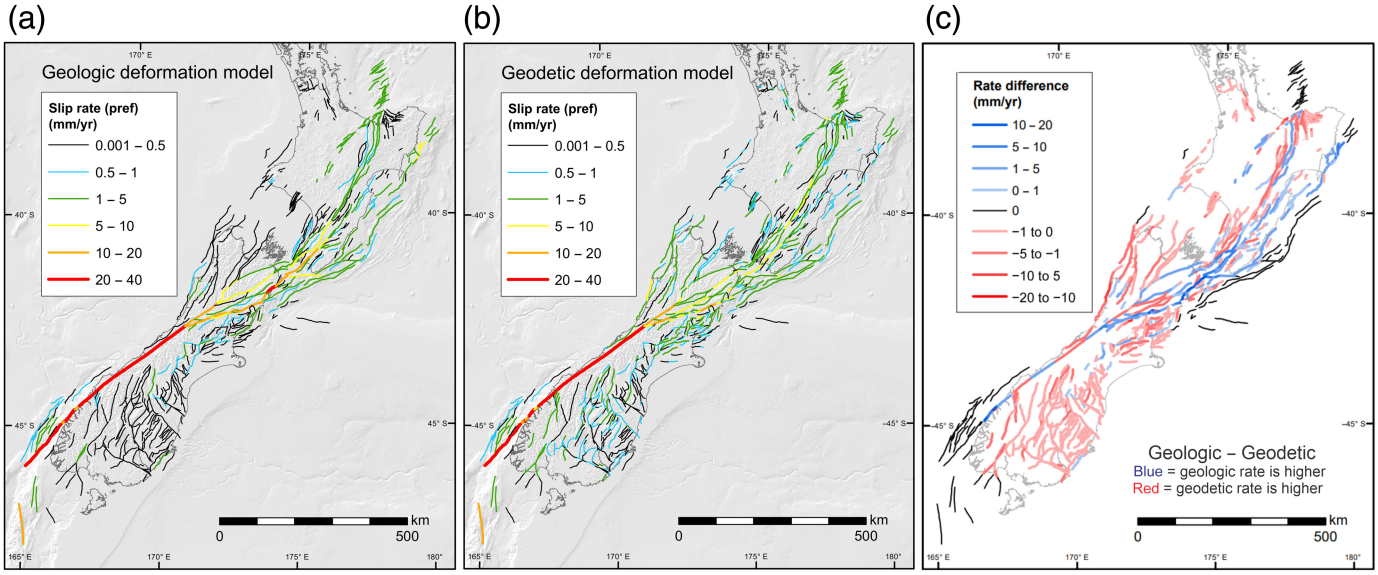

Figure 9. Map views of the New Zealand National Seismic Hazard Model (NZ NSHM) 2022 upper-plate deformation models with fault traces color-coded by preferred slip rate. (a) Geologic deformation model; and (b) geodetic deformation model. The rates depicted in the geodetic deformation model are the preferred depth-averaged slip deficit rates derived from the median of the four best-fitting slip deficit rate inversions—one inversion for each strain-rate map. In addition, geodetically unconstrained slip deficit rates for offshore faults have been replaced with the geologic deformation model slip rates. (c) Map portraying the difference between the preferred geologic slip rates of the geologic deformation model and the mean depth-averaged slip deficit rates of the geodetic deformation model. The blue colors denote that rates are higher in the geologic deformation model compared with the geodetic model, and the red colors denote higher rates in the geodetic deformation model. The color version of this figure is available only in the electronic edition.

hazard resulting from use of either of the two models so, for the sake of computational efficiency, only a single model (the "locked to trench" rendition) was chosen for final use in the NZ NSHM 2022 (Fig. 10a).

Development of the Puysegur subduction interface deformation model is presented in Van Dissen *et al.* (2022, 2024). Its geometry is taken directly from the NZ CFM v.1.0 adopting a "cut by the Alpine fault" interpretation, and its slip deficit rate is derived from plate convergence rate and interface coupling considerations (Wallace *et al.*, 2007; Fig. 10b).

Rupture sets

Multifault ruptures are common for historical earthquakes in New Zealand and internationally (e.g., Kurushin *et al.*, 1997; Fletcher *et al.*, 2016; Litchfield *et al.*, 2018; Nicol *et al.*, 2022). These complex rupture geometries have been incorporated into the NZ NSHM 2022. UCERF3 was the first seismic hazard model to systematically include multifault earthquakes using rule sets (Milner *et al.*, 2013; Field *et al.*, 2014). The NZ NSHM 2022 uses the workflow established in UCERF3 in which plausibility filters provide the rules governing whether adjacent faults or fault sections could rupture together and fault-slip rates constrain the participation rate of these ruptures (i.e., the frequency of each rupture geometry).

Using the fault geometries and locations in the upper-plate deformation models, and applying the 15 km maximum jump distance and the plausibility filter of Milner *et al.* (2022), 232,906 unique ruptures are considered plausible and have been included in the NZ NSHM 2022 rupture set. The population of rupture lengths range between <50 and ~1200 km, with a mode of ~375 km. The number of ruptures >800 km decreases rapidly, whereas the longest ruptures typically represent "wall-to-wall" ruptures that incorporate the Alpine fault, Marlborough fault system (MFS), and North Island dextral fault belt. By reducing the maximum jump distance to 1 km these wall-to-wall ruptures can be removed from the rupture set, decreasing the maximum rupture length to ~800 km (e.g., Alpine fault and MFS).

Although considered plausible (based on the rules used), wall-to-wall ruptures occur infrequently. Gerstenberger, Van Dissen, *et al.* (2022) showed that rupture lengths of >900 km typically occur once every 50,000 yr. By contrast, ruptures with lengths of 50–100 km occur every 80–100 yr. Ruptures with lengths of <350 km are within an order of magnitude of the rates of historical earthquakes, although it is acknowledged that at ~180 yr this historical record is short by comparison with the >1000 yr recurrence rates for lengths of >300 km in the IFM.

The rules governing rupture set construction for the subduction interfaces in the NZ NSHM 2022 are much simpler than those for the upper-plate faults. For the subduction interfaces, ruptures are constrained to have a length-to-width (L:W) aspect ratio of between 1:1 and 5:1 until the full down-dip width of the interface is occupied; then ruptures can grow in length unbounded.

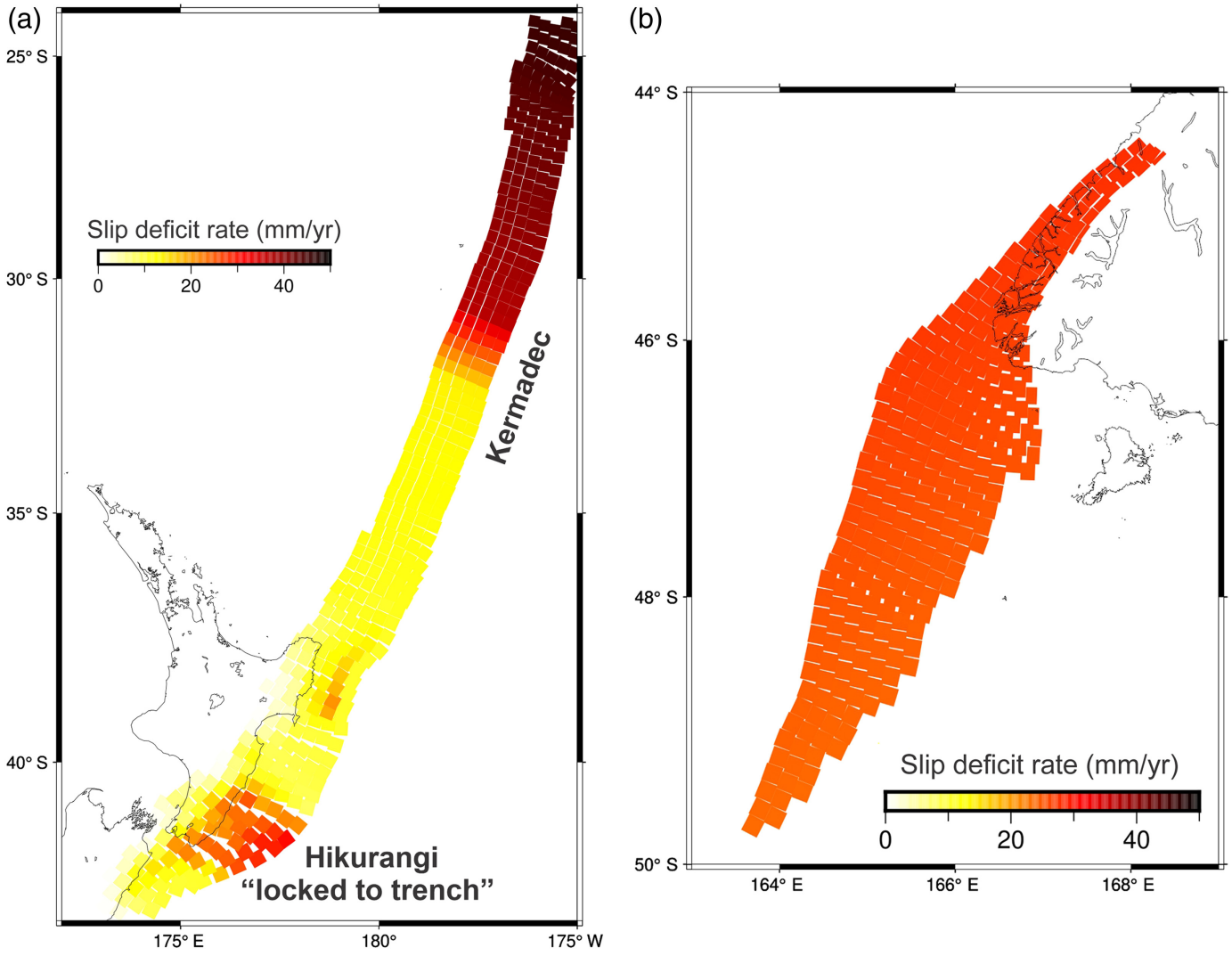

To reduce computational demands, and in a fashion similar to construction of the upper-plate fault rupture set, plausible interface ruptures are passed through the "Adaptive Rupture Growing Strategy" filter to remove ruptures from the rupture set that have similar total subsection counts (i.e., with geometries and areas that are similar). In total, there are 23,675 ruptures in the Hikurangi–Kermadec subduction interface rupture set and 15,800 ruptures in the Puysegur interface rupture set.

Fault polygons

We have applied a simplified implementation of fault polygons based on what was applied in UCERF3 (Powers and Field, 2013). Fault polygons serve a primary function of being a tool for combining the DSM and IFM, and they are used to determine the on-fault/off-fault ratio of forecast seismicity to scale the overall *N*-value to create the MFD target for the inversion as part of this. The polygons are created in 3D using a buffer of 12 km around the fault surface; see figure 02c of Powers and Field (2013). UCERF3 applied a dip-based buffer width, which tapered from 12 km at 90° dip to 0 km at 50° dip; however, they combined the distance-based buffer with a subjectively defined

Figure 10. Subduction interface deformation models of the NZ NSHM 2022. (a) Hikurangi–Kermadec subduction interface deformation model. The slip deficit rate for the Kermadec portion of the interface is based on the convergence rates of Power *et al.* (2012) and applying the following coupling coefficients: 0.2 south of 32.5° S, 0.5 north of 31° S, and a linearly increasing transition zone from 0.2 to 0.5 between 32.5° S and 31° S. In the NZ NSHM 2022, the Hikurangi–Kermadec subduction interface deformation model surface is discretized into adjoining 30 km × 30 km quadrilateral patches. (b) Puysegur subduction interface deformation model. Slip deficit rate of the Puysegur interface is based on the AUS/PAC Euler pole of rotation presented in Wallace *et al.* (2007), and a coupling coefficient of 0.7 is adopted based on the Global Earthquake Model coupling coefficient listed in Christophersen *et al.* (2015) (which was based on interseismic coupling models of the Puysegur trench from Wallace *et al.*, 2007). This yields a slip deficit rate on most of the interface of ~27 mm/yr. For use in the inversion fault model (IFM), the Puysegur interface is discretized into 15 km × 15 km patches. The smaller patch size, compared with the Hikurangi–Kermadec interface, was needed to accurately represent its geometry. Note that the slip rate color scale in both the panels is the same but the geographic scale is not. Compared with the Hikurangi–Kermadec deformation model depicted in panel (a), the Puysegur model in panel (b) is shown at ~2× magnification. The color version of this figure is available only in the electronic edition.

geological buffer, which typically had the minimum width of 1 km. We have chosen to keep the polygon definition as simple as possible and to remove an additional decision from polygon definitions. Therefore, we use a 3 km minimum distance for shallow dipping faults, that is, for dips of 50° or less we apply a buffer of 3 km to the surface projection of the fault in the up- and down-dip directions. This is applied to account for the lack of spatial precision of geometries of some faults in the network and to allow for the inherent uncertainty in what is considered on-fault and off-fault in the construct of the IFM.

Earthquake recurrence interval and probability of detection

In a fashion similar to UCERF3, the NZ NSHM 2022 uses recurrence intervals derived from paleoseismic data as one constraint of many to solve for rates of fault ruptures. These recurrence intervals derivations are detailed in Coffey *et al.* (2022, 2024) and use a weighted combination of recurrence time distributions, including lognormal, Brownian Passage Time, and Poisson.

In NZ NSHM 2022, the maximum-likelihood mean recurrence intervals are derived using three different approaches based on methods previously applied in UCERF3 (Biasi, 2013; Madden *et al.*, 2013; Weldon and Biasi, 2013) and by Rhoades and Dissen (2003), Rhoades *et al.* (2011), and Van Dissen *et al.* (2013) for active faults in New Zealand. These methods utilize earthquake timing and SED data from the New Zealand Paleoseismic Site Database (Litchfield *et al.*, 2022, 2024) and geologic-based slip-rate data from the NZ CFM v.1.0 (Seebeck *et al.*, 2022, 2023) and geodetic-based slip-rate data drawn from the NZ NSHM 2022 geodetic deformation model (Johnson *et al.*, 2022, 2024; Van Dissen *et al.*, 2022, 2024). The three methods are described in detail in Coffey *et al.* (2022, 2024) but broadly include: (1) the earthquake-timings-only method, where earthquake ages have been measured for three or more events (Biasi, 2013); (2) the SED divided by slip rate (SED/SR) method, where a fault has three or more SED measurements and a robust slip rate (Madden *et al.*, 2013); and (3) the Rhoades and Van Dissen (R&VD) method for sites where all the above data are available (Rhoades and Dissen, 2003; Rhoades, Van Dissen, *et al.*, 2011). Sites from the Paleoseismic Site Database were interrogated to identify those with sufficient data for recurrence interval analysis, and each recurrence interval derivation method is applied based upon the availability and quality of the relevant paleoseismic data. Where multiple methods can be applied, the results are incorporated in decreasing order of priority as follows: the R&VD method (3), the earthquake-timings-only method (1), and then the SED/SR method (2), as this order reflects a decrease in number of geological constraints.

For the NZ NSHM 2022, recurrence intervals were derived for 81 locations using one or all three of the methods described earlier and range from as short as a couple of hundred years to as long as several tens of thousands of years. Mean recurrence intervals and their confidence intervals for all faults evaluated as part of NZ NSHM 2022 can be found in Coffey *et al.* (2022, 2024).

Following the lead of UCERF3, the NZ NSHM 2022 uses paleoearthquake timing information (expressed as recurrence intervals) to constrain inversion-based hazard results. Consequently, it is important to understand what proportion of "real-world" earthquakes are reflected in the paleoseismic record used to derive recurrence intervals and, related, to understand what subset of all ruptures in the crustal rupture set that a specific subsection is involved in is comparable to the "real-world" earthquake timings (and derived recurrence intervals) at paleoearthquake sites located on that subsection. This issue is addressed in Weldon and Biasi (2013) who present a methodology to derive the probability of detection of ground rupture at paleoseismic sites. The NZ NSHM 2022 adopts the general methodology detailed in Weldon and Biasi (2013) to determine, as a function of earthquake magnitude, the probabilities that surface ruptures will be detected at paleoseismic sites both for the TVZ and for the rest of the New Zealand region outside of the TVZ. The method has been amended to be consistent with New Zealand earthquake data (including New Zealand-specific estimations of likelihood of surface rupture) as a function of magnitude (e.g., Nicol, Van Dissen, *et al.*, 2016) and specific magnitude–area scaling relations already used elsewhere in the earthquake-rate calculations undertaken within the NZ NSHM 2022. Details of these calculation are found in Coffey *et al.* (2022, 2024). Compared with UCERF3 results, New Zealand earthquakes outside of the TVZ appear to be significantly less "detectable" than comparable earthquakes in California (Fig. 11), whereas earthquakes in the TVZ appear to be more "detectable" than similarly sized earthquakes in California.

Conditional probability of rupture

Conditional probability of rupture is incorporated into the UCERF3 stable of rupture rate hazard forecasts through the methodology detailed in Field *et al.* (2015). This methodology adopts a Brownian Passage Time recurrence distribution with a magnitude-dependent aperiodicity. It uses the earthquake rupture rates (recurrence intervals) generated from the inversion solutions and most recent event (i.e., last event) timing constraints that are either known historically through paleoseismic investigations or only loosely constrained to be prehistoric. To incorporate conditional probability of rupture into a component of NZ NSHM 2022, we have adopted the UCERF3 method of (Field *et al.*, 2015). However, instead of applying this to all faults (fault sections and subsections) in the crustal deformation models, as was done in UCERF3, we, due to project time constraints, apply the conditional probability methodology only to the faults that would potentially experience the greatest change in rupture rate compared with their

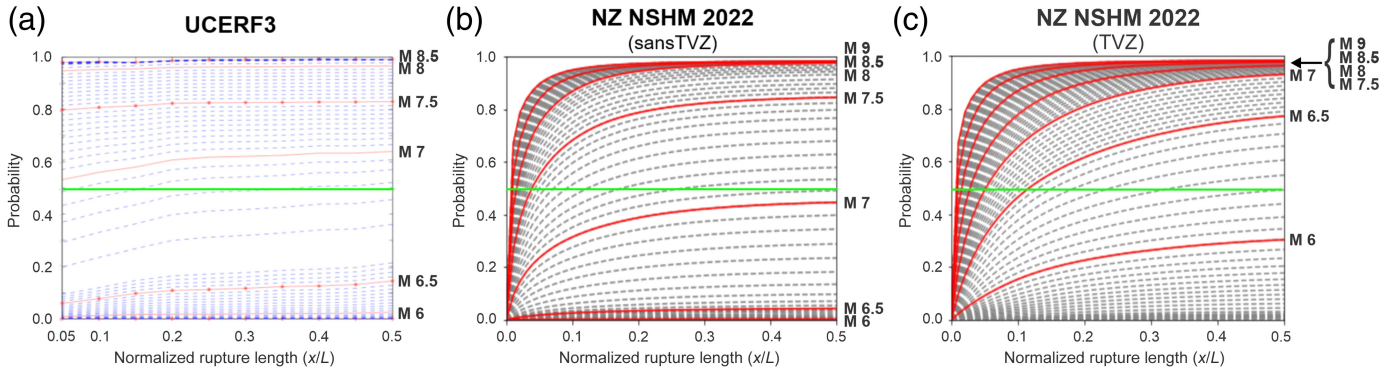

Figure 11. Comparison of probability of paleoearthquake detection curves as a function of magnitude and position (*x*/*L*) along a rupture. (a) UCERF3 (Weldon and Biasi, 2013, their fig. I9); (b) sansTVZ New Zealand; and (c) the Taupō Volcanic Zone (TVZ) New Zealand region. sansTVZ refers to the region of New Zealand outside of the TVZ. The plot shows the combined effect of the probability of the earthquake having produced surface rupture and the probability of the event being detected at a "trench" site. Each set of curves is plotted at the same scale and, for reference, has a horizontal green line scribed at 0.5 probability of detection. The color version of this figure is available only in the electronic edition.

Poissonian rate. Put another way, in NZ NSHM 2022, we apply the conditional probability of rupture methodology only to those faults that will potentially experience the greatest probability gains or losses by considering timing since their most recent event. These are almost invariably the faults with the shortest recurrence intervals (or highest slip rates) and/or those that have ruptured most recently. In the conditional probability component of NZ NSHM 2022, we have chosen to include about 90 fault sections with a preferred slip rate in the geologic deformation model of ≥4 mm/yr or those that have ruptured since 1840 C.E. (i.e., within the colonial historic period). This set of faults includes the high-slip-rate Alpine fault, most of the major faults within the MFS (e.g., the Wairau, Awatere, Clarence [most of it anyway], Hope, Kekerengu, and Needles faults), and the high-slip-rate faults of the North Island dextral fault belt (including the Wairarapa and Wellington faults). The historic rupture component of the criteria ensnares slower slip-rate faults that ruptured in, for example, the 2016 Kaikōura earthquake (e.g., The Humps, Leader, and Hundalee faults), the 2010 Darfield earthquake (Greendale fault), and the 1931 Hawke's Bay earthquake (Poukawa and Awanui faults). There are about 500 fault sections in the geologic deformation model that have slip rates less than 4 mm/yr. For these faults, in the conditional probability component of NZ NSHM 2022, a most recent event timing of ≥180 yr was universally applied. This pragmatic choice is of little consequence from an overall hazard perspective.

A more significant difference is that the aperiodicities adopted in the NZ NSHM 2022 are noticeably higher than those used in UCERF3. For example, 0.5 is the aperiodicity that used NZ NSHM 2022's highest magnitude bin; whereas 0.1–0.3 is the range of Brownian Passage Time aperiodicities used in UCERF3's highest magnitude bin. We consider that the higher aperiodicities adopted in NZ NSHM 2022 are warrant based on: (1) the findings of Biasi *et al.* (2015) who derived a recurrence interval aperiodicity of 0.44 for more than 20 paleoearthquake event records at Hokuri Creek on the Alpine fault; (2) the findings of (Nicol, Robinson, *et al.*, 2016) who derived an average aperiodicity for New Zealand faults of 0.6 ± 0.2; and (3) the findings of Griffin *et al.* (2020) who concluded that the recurrence intervals of fast slipping active faults are only weakly to moderately periodic (implying an aperiodicity of 0.5–1.0). A consequence of adopting higher aperiodicities (compared with lower ones) is that probabilities start to rise sooner following a rupture, but more gently, and they do not reach as high a peak.

IFM results

Crustal IFM. Figures 12 and 13 show example solution fits for the geological deformation model with the best goodness of fit with $b = 0.82$, $N = 2.7$, and $c = 4.2$. Both the figures demonstrate the nature of the method and solutions in that multiple datasets are jointly fit. Shown are the misfits of the final solution versus two input constraints: slip rate and MFD. The misfits are the results of the joint influence of constraints including the available ruptures in the rupture set, the geological deformation model slip rates, the MFD, the recurrence intervals of known past events, and along-strike smoothing of the MFD. The largest misfits in the slip rate tend to be controlled by the recurrence interval constraints. An example of this can be seen for sections on the Alpine fault, which have a target slip rate of about 24 mm/yr and solution slip rates of 26–30 mm/yr.

Figure 14 shows an example of along-strike variation in the rate at which fault sections participate in rupture. This figure shows sections of the Wellington fault and compares it with the geologically determined occurrence rate showing that the fit is within this uncertainty. We note that in many inversions, especially those using the upper-plate geologic deformation model, even when slip-rate fit may be perceived to be poor, the fit to paleoearthquake timing recurrence intervals was invariably within the uncertainties of that recurrence interval data. This means that even when the fault-slip rate was not being

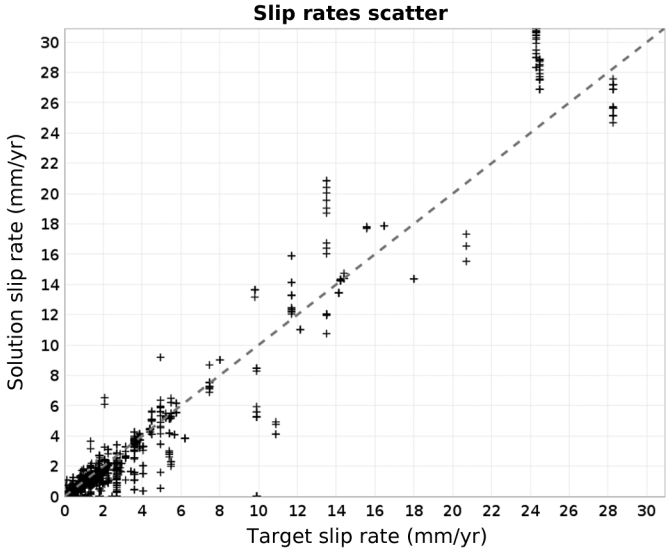

Figure 12. Slip-rate fits from one heavily weighted logic tree branch. The *X*-axis is the slip rate from the geological deformation model, the *y*-axis is the solution slip rate ($N = 2.7$, $b = 0.82$, scaling relation $c = 4.2$, inversion solution weight = 1). This solution contains 1,736 ruptures with a supraseismogenic rupture rate of 22 yr. The companion magnitude–frequency distribution (MFD) is shown in Figure 13.

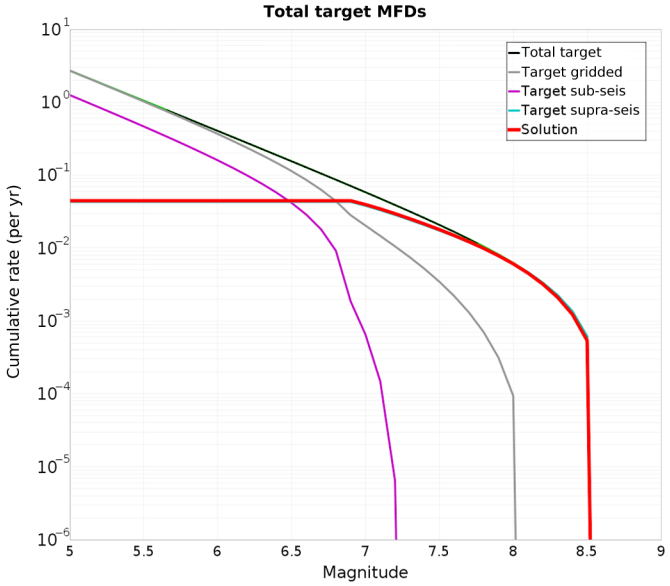

Figure 13. The MFD fit corresponding to the slip-rate fits in Figure 12. The target rate ("Total target") is shown in green, and the solution is shown in red. Target Gridded (gray) shows the total distributed seismicity model (DSM) MFD. The purple and cyan break down the combined IFM and DSM rates into ruptures that are smaller ("Target sub-seis") than those modeled in the IFM ($M_w \lesssim 6.9$) and those that are greater than M_w 6.9 ("Target supra-seis"), respectively. The solution curve obscures the target supraseismic curve, because the fit to the MFD constraint is quite good in this example. The color version of this figure is available only in the electronic edition.

fit well, the specific fault section was still involved in large earthquakes at a rate consistent with the recurrence interval constraints. We are comfortable with this apparent inconsistency because: (1) in many cases the timings data are better constrained than the slip-rate data; (2) the aleatory variability in the scaling relations is not directly accounted for, and this can impact the consistency of the recurrence rate and slip rates estimated from SEDs (this may be particularly important for faults which rupture jointly with the subduction interface, which we do not currently model); and (3) it is the rate of earthquake occurrence that is most relevant (not fit to slip rate) from a hazard perspective.

Hikurangi–Kermadec subduction inversion results. For the Hikurangi–Kermadec subduction interface, we show a representative example of the "locked to trench" results; the "creeping at trench" results are nearly identical. The results are shown for *b*-value = 0.95 and *N*-value = 17.5 (Fig. 15) and for the MFD models (Fig. 16) that have better fits when compared with the alternative models. This is reflected in a five times higher inversion solution weight calculated for the *b*-value = 0.95 solution. The moment rate difference across the two models is <4%.

Puysegur subduction inversion results. For the Puysegur subduction interface IFM, when using $C = 4.0$, only one *b*- and *N*-value pair produces what is considered a credible model, and only this model is proposed to be used. The use of other magnitude–area scaling relation *C*-values does produce credible alternatives, but the exploration of the impact of different *C*-values on hazard is left to future NSHM revisions.

COMBINING THE DSM AND IFM

The previous NZ NSHMs (Stirling *et al.*, 2002, 2012) have done an additive combination of the DSM with the fault model. This creates the possibility that the same earthquake is forecast in both the models, creating a potentially conservative hazard estimate. If this conservatism is present, it may be seen in a bulge in the MFD in the magnitude range that overlaps between the fault model and the DSM. Other NSHMs, including UCERF3 (Field *et al.*, 2014; Gerstenberger *et al.*, 2020), handle this potential conservatism (i.e., a potential overforecast) by truncating the background rates at the minimum fault magnitude in regions near faults; this solution assumes that all forecast rates in the overlapping magnitude bins are forecast by both the model components resulting in a complete double forecast of these rates. Although it is very likely that there is some amount of double forecast, the true amount is unknown. This solution potentially removes rates that are not double forecast in both the models and removes the epistemic uncertainty modeled by the alternative forecast provided by the DSM. In other words, such a truncation expresses a degree of belief of 0 for the magnitudes considered; this is contrary to what we have outlined in the Forecast time

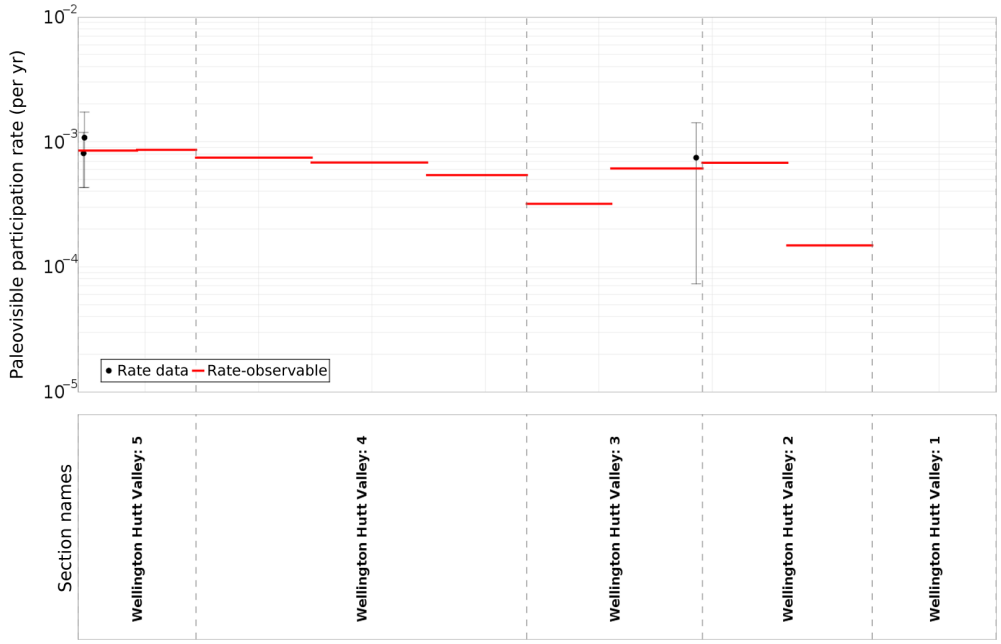

Figure 14. The along-strike variation in rate for which individual sections of the Wellington fault are modeled to participate in ruptures from one model run (red). Also shown (black dots) are the geologically determined recurrence intervals with uncertainty, which are also used to constrain the solution. We note the absence of rates on Wellington Hutt Valley: 1; this solution preferred to place the rates onto the very nearby Ohariu fault. This model uses the geological deformation model, $N = 3.4$, $b = 0.96$, and scaling relation $C = 4.2$. The color version of this figure is available only in the electronic edition.

window section. The DSM in the 2022 NZ NSHM is conceptually different from DSMs used in other NSHMs in that it combines multiple models and datasets. On its own, the DSM provides a credible alternative to the IFM for all magnitudes; hence, we used the following method for combining the models to retain some of the forecast skill of the DSM for larger magnitudes. For multiple reasons, but most importantly, because the IFM does not forecast all magnitudes, we cannot apply the IFM and DSM as independent branches in the logic tree, and we must combine them. Therefore, we apply a spatially tapered weighting function to the DSM within the fault polygons. The function weights the DSM 100% at the boundaries of the polygon and uses a power law taper to 0 at the fault location; the DSM grid is up-sampled just for this calculation (Fig. 17). The fault model is down weighted to accommodate the weighting applied to the DSM. We apply an 80% weight to the IFM and a 20% weight to the DSM for magnitudes greater than M_w 6.7 (i.e., greater than the M_{min} in the IFM) inside the polygons.

HAZARD SENSITIVITY TESTING AND TRIMMING THE LOGIC TREE

To reduce the number of logic tree branches (Figs. 1–3), sensitivity tests were done to identify parameter options that had no meaningful impact on the results (Gerstenberger, Bora, *et al.*, 2022; Gerstenberger *et al.*, 2024). The motivation to reduce the size of the logic tree was primarily not only to improve calculation time but also to reduce unnecessary complexity of the model. It was not possible to use strict criteria to judge the need for retaining a parameter choice because of the many subjective considerations required. For the hazard sensitivity testing, the relative impacts of a parameter choice on the many uses of the model, when compared with other parameters, were considered. The list of comparative considerations included but was not limited to mean and higher fractile hazard, impact relative to the effect of the GMCM, and influence on the distribution of low-probability high-impact ruptures. Because NZ NSHMs have many uses, other considerations aside from hazard impact, such as the need to provide deformation models that show the uncertainty in our knowledge of slip rate, were important in the logic tree trimming process. An absolute metric for comparison would be ideal, but this is the subject of future work. Doing so may be challenging, given the many and varied uses of hazard forecasts.

Hazard sensitivity tests were done as a combination of hazard curves and maps. The hazard curves were calculated for 35 key cities around New Zealand; these represent a range of tectonic regions and seismicity rates, and cover most of the country (Gerstenberger, Bora, *et al.*, 2022; Gerstenberger *et al.*, 2024). The hazard curves were investigated for peak ground acceleration, spectral acceleration, SA(0.5 s), SA(1.5 s), and SA(5.0 s). The format of the sensitivity tests was, for example, to choose a single deformation model coupled with a representative suite of the other source model components. A full preliminary GMCM logic tree that was available at the time was used (Bradley *et al.*, 2022, 2024). This consists of uniformly weighted Next Generation Attenuation-Subduction (NGA-Sub) models (excluding NZ-specific adaptations) for the subduction interfaces, and for crustal 0.5 weight was given to Stafford (2022), and, 0.5 was given uniformly to the selected suite of NGA2-West and Bradley (2013) models, as explained in Bradley *et al.* (2022, 2024). The resultant hazard curves were all plotted in a single plot and parameter sets were identified.

In addition, and for risk considerations, the impact on the complexity and length of ruptures was considered through

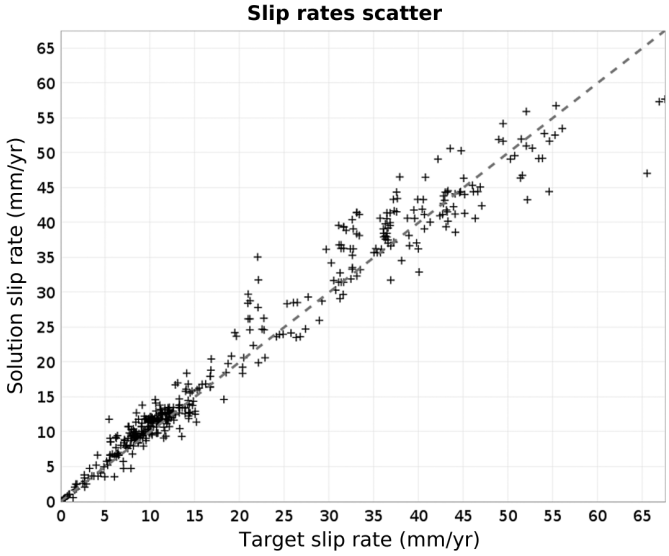

Figure 15. Slip-rate fits from one Hikurangi–Kermadec logic tree branch. The *X*-axis is the slip deficit rate from the deformation model; the *y*-axis is the solution slip rate ($N = 17.5$, $b = 0.95$, scaling relation $c = 4.0$). This solution contains 1318 ruptures. The companion MFD is shown in Figure 16.

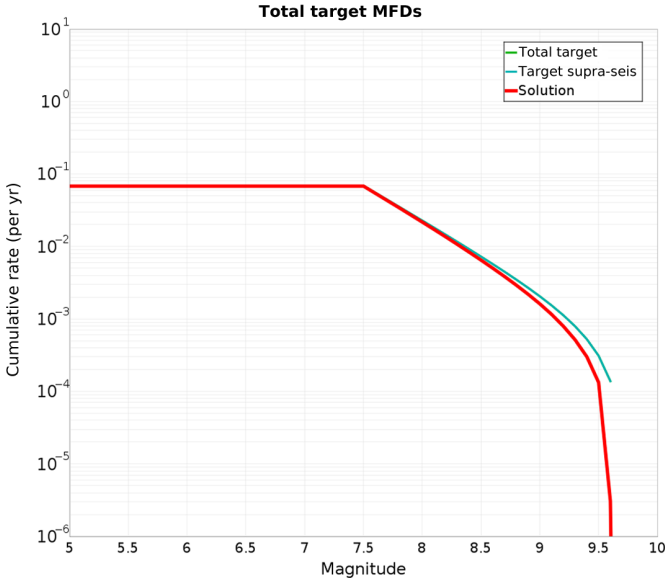

Figure 16. The MFD fit corresponding to the slip-rate fits in Figure 15. The target rate ("Total target") is shown in green, and the solution is shown in red. "Target supra-seis" (cyan) is identical to the total target, because there is no DSM removed from the target MFD for subduction interface inversions. The color version of this figure is available only in the electronic edition.

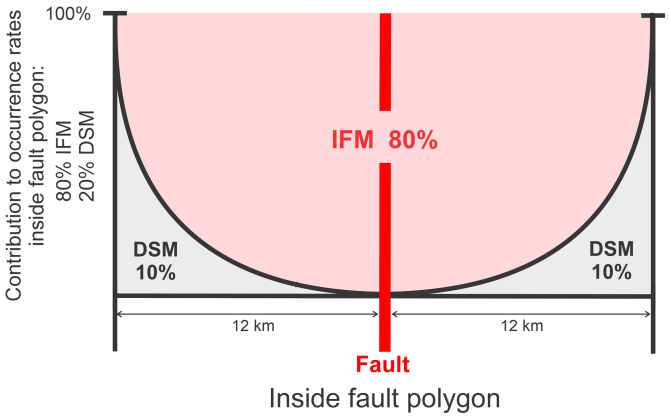

Figure 17. Schematic illustration of how the DSM occurrence rates and IFM rates is combined within a fault polygon. The color version of this figure is available only in the electronic edition.

informal analyses of the ruptures assigned nonzero rates. For example, we examined the different parameter solutions for changes in distribution or rates of large crustal earthquake ruptures, which may impact multiple population centers.

In the development of many of the component models, coarse sensitivity tests were done to reduce initial model options. For final sensitivity testing, four options were tested: (1) magnitude–area scaling relation parameter C; (2) maximum rupture jump distance; (3) crustal deformation model; and (4) *N*-value.

Crustal sensitivity testing

Hazard was not sensitive to the choice of magnitude–area scaling relation parameter *C*, allowing only a single value to be used in the final logic tree ($C = 4.2$). Similarly, changing the maximum rupture jump distances of 3, 5, 10, and 15 km only had small impacts in isolated locations and were not considered meaningful relative to other changes. Of note was increased connectivity between the TVZ and the North Island dextral fault belt and in the Gisborne region, which also impacted hazard at PoE of $<10^{-4}$. The increased connectivity allowed for ruptures to, for example, jump across the Okataina Caldera. The possibility for such ruptures is poorly constrained and cannot be ruled out. As shown in Figure 1, a single jump distance value of 15 km was chosen. Finally, the choice of *N*-value and *N*-value scaling branches showed large differences in hazard (Gerstenberger, Bora, *et al.*, 2022; Gerstenberger *et al.*, 2024), and all were retained.

As discussed in the DSM section, extensive sensitivity testing in both occurrence rate space and hazard space was performed during the development of the DSM (e.g., Iturrieta *et al.*, 2022; Rastin *et al.*, 2022; Rollins, Gerstenberger, *et al.*, 2024). In addition, although the DSM does use the traditional logic tree concept to explore epistemic uncertainties, the core of the model is a hybrid. Traditional PSHA models and the combination of DSMs with fault-based models can also be considered a form of hybrid, that is, a joint forecast of the two components is developed rather than alternative forecasts from the two models. In the NZ NSHM 2022, the DSM has two stages of hybridization: first, the so-called hybrid model is developed, and, second, the final hybrid model is developed by combining this with the URZ model. The philosophy is that the optimal model and forecast are developed through a

TABLE 6
Moment-Rate Comparison between 2010 and 2022 National Seismic Hazard Models (NSHMs) Fault Sources

Model Component	Total Moment Rate (N·m/yr)	Total Area (km^2)	Average Slip Rate (mm/yr)
Upper-plate (crustal) fault models			
2010 active fault earthquake source model	2.17×10^{19}	294	2.5
2022 geologic deformation model	2.89×10^{19}	446	2.2
2022 active fault earthquake source model	2.99×10^{19}	446	2.2
Hikurangi subduction interface models			
2010 Hikurangi interface	1.85×10^{19}	75,000	8
2022 locked to trench: 2010 extent	5.26×10^{19}	161,000	10.9
2022 locked to trench: full 2022 extent	2.56×10^{20}	406,800	21.0

For crustal faults, the single 2010 model is compared with the geological and geodetic deformation models from 2022. For the Hikurangi interface, only the deformation model used in the final logic tree is shown. The modeled extent of the 2022 Hikurangi–Kermadec interface is considerably farther north than the Hikurangi interface in 2010. For this reason, an additional comparison is shown, which truncates the 2022 model in a similar location as the 2010 model.

statistical combination of components models. Following sensitivity analyses it was considered that differences across models were not meaningful, given the criteria developed above; therefore, a single hybrid model has been used. Further exploration of epistemic uncertainty related to the hybrid model can be performed by systematically exploring the influence of different weighting schemes and the uncertainty in the weights provided during the elicitation process (e.g., Gerstenberger *et al.*, 2016; but this is left for future work.

Hikurangi–Kermadec sensitivity testing

The results of the sensitivity tests for the "locked to trench" and "creeping at trench" deformation models show almost no difference across all locations. Differences only become apparent in a few locations at the annual PoE of $<10^{-4}$. The differences indicate that the use of two slip deficit rate models of the Hikurangi–Kermadec interface is not warranted due to the additional computational expense and complexity it brings to the model.

Overall, relatively small differences are seen across the three magnitude–area C-values of 3.9, 4.0, and 4.1. In Hawkes Bay and Gisborne, slightly larger differences are seen, which may potentially justify including multiple values. However, given the larger impact on the mean and uncertainty range from other SRM and GMCM parameters and the overall poorer fit in the inversions from 3.9 and 4.1, we have opted to include only the consistently best-fitting C-value of 4.0.

MOMENT-RATE COMPARISONS WITH THE NZ NSHM 2010

The NZ NSHM 2022 includes substantial revisions of all components of the model when compared with the NZ NSHM 2010 (Stirling *et al.*, 2012). This makes a direct and quantitative comparison of the component models challenging to do. Nevertheless, there are some informative comparisons that can be made. Table 6 shows a comparison of the slip-rate-derived moment rate available for earthquakes modeled on known faults in both the NZ NSHM 2022 and the NZ NSHM 2010. For the 2010 NSHM, this translates directly to the forecast moment rate. For the 2022 NSHM the slip rate is not the sole controller of the forecast moment rate, and it is balanced in the inversion with the overall MFD and the timings of past earthquakes. This results in a forecast of 1.08×10^{19} N · m/yr to 2.72×10^{19} N · m/yr without N-scaling. An additional complication for the interface comparisons is that much larger areas are modeled in the 2022 NSHM for both the Hikurangi interface, and these changes dominate any comparison. The larger areas are related to the greater depth extent in the 2022 model (up to about 60 km depth for 2022, and ranging between 15 and 30 km for 2010) and due to both 2022 interface models extending to the seabed, whereas the 2010 model extends to 5 km depth. This is the case for both the locked and creeping at trench models. The NZ NSHM 2022 forecast moment rate for the Hikurangi–Kermadec interface ranges from 7.43×10^{19} N · m/yr to 2.28×10^{20} N · m/yr without N-scaling.

For the crustal model, both the geodetic and geologic deformation models are more than a 25% increase in available moment rate. This results in a range of forecast moment rates that, without N-scaling, range from about a 50% decrease to a 25% increase. The application of the N-scaling increases this difference range proportional to the factors shown in Table 3, for example, by ∼25% again in each direction. For the Hikurangi portion of the Hikurangi–Kermadec, the 2022 slip deficit model represents about a three-times increase in moment rate. The complete Hikurangi–Kermadec interface is more than a 10 times increase. This results in a range of forecast moment rates that are increased from 4 to more than 10 times; to be clear, this is when the entire 2022 Hikurangi–Kermadec interface is compared with the 2010 Hikurangi interface.

Similarly to the IFM, the 2022 DSM is a different modeling construct from the 2010 DSM. The most informative comparison is of the total moment rate for each model, including the crustal, interface, and slab DSM components. Comparisons of subcomponents are not meaningful due to the significant differences in concepts. The moment rate for the 2022 DSM is 1.8×10^{19} N · m/yr and 7.9×10^{18} N · m/yr for the 2010

DSM. This is an increase by a factor of more than 2 in the 2022 DSM. The dominant contributors to this are: (1) increases in the maximum magnitude for crustal events from 7.2 in 2010 to 8.0 in 2022; (2) from 7.2 to 7.5 for the Hikurangi interface (with no DSM being modeled for the Kermadec portion); and (3) from 7.2 to 8.15 for the subducting slab. An additional increase comes from slab events that are modeled down to 250 km in 2022 compared with 100 km in 2010. Approximately half of the slab moment in 2022 comes from below 100 km. Finally, and counteracting some of the aforementioned increases is the decrease in moment rate in 2022 that comes from the use of the earthquake catalog that has been homogenized to M_w. This compares to the 2010 DSM, which was derived from a catalog containing a significant percentage of M_L events. The M_L are consistently larger than their equivalent M_w, and their use results in increased occurrence rates for the same observed earthquakes (Christophersen *et al.*, 2024).

CONFIDENCE AND UNCERTAINTY

As part of the development of the SRM we constructed and regularly updated an uncertainty matrix (Gerstenberger, Van Dissen, *et al.*, 2022). The format of the matrix evolved throughout the course of the project. This matrix was for internal auditing to help us establish confidence that we have covered relevant uncertainties and parameters to help guide eventual logic tree weighting, and it has been used to communicate the confidence the modeling team has across the many key uncertainties of the model. All metrics were subjectively weighted by the SRM team in multiple revisited informal consensus processes. In the assessment process, all uncertainties were considered, including those that are currently not well constrained or able to be modeled. For example, a poorly constrained or understood uncertainty was given a low confidence. A simplified summary of the full matrix is shown in Figure 18. This figure has been used for communicating with key users of the NZ NSHM 2022 the confidence in key parameters.

RECOMMENDATIONS FOR FUTURE IMPROVEMENTS

The approximately two-year timeframe for the 2022 NZ NSHM revision was a significant undertaking with a large amount of research and modeling completed in a limited time. As with any such project, decisions were required, and research could not be continued indefinitely; therefore, several SRM challenges were identified that can be improved upon in the future revisions. The NZ NSHM 2022 is expected to be the first in an ongoing revision cycle.

Some key limitations and identified areas for improvement in the future NZ NSHM revisions include:

Overall Model

- Sensitivity tests were done with models and information that were available at the time the test was performed. Where possible, these have been redone with later iterations of the model. We do not have evidence to suggest that this impacts any results, but future work could pursue a more detailed exploration of the sensitivity to model choices and further refinement of the logic tree.
- We did not fully explore epistemic uncertainty in the method of combining the DSM with the IFM. Sensitivity tests indicated that this was not a significant source of uncertainty within the current implementation, but the future work is required to improve understanding of the different datasets, models, and how they can be combined.
- The crustal and interface IFMs have been treated independently. The future versions should consider the potential for joint ruptures of the interface and crustal sources as was likely in the 2016 Kaikōura earthquake and the 1855 Wairarapa earthquake. This requires future work in identifying both temporal and spatial constraints on such ruptures.

Crustal Model

- Improvements to the simulated annealing inversion implementation should be explored to allow for improved quantification of the uncertainty space and improved identification of the range of potential rupture rates, including low-probability high-impact ruptures.
- Improved understanding should be developed of the trade-offs between and implications of fitting *N*-value, *b*-value, slip rate, and paleoearthquake timings and scaling relations in the inversion solutions.
- Further consideration of key fault parameters, including dip, depth to bottom of rupture, potential for interfault connectivity, and the minimum rupture magnitude considered for the inversion. Better constraints on the slip-rate uncertainty for both the geodetic and geologic deformation model are required as is more focused exploration of alternative deformation models. This includes any implications of the spatial resolution of the geodetic models and the ability to distinguish closely spaced faults, such as in the Wellington region. For both deformation models, future work is required to understand what amount of nonseismogenic slip may be present in the estimated slip rates.
- The Taupō rift–Havre trough contains a complex network of exceptionally closely spaced shorter faults where their connectivity at depth is poorly understood but likely to be significant. To handle this uncertainty, in the NZ NSHM 2022, faults with slip rates of <1.8 mm/yr were modeled in the DSM (including use of their slip rates), and faster faults were modeled in the IFM. Future work is required to: (1) better understand the connectivity of faults at depth and (2) develop an improved method to model ruptures in this region.
- Future work should pursue a more encompassing and nuanced treatment of fault-rupture time dependence, including application to all suitable faults (not just those with slip rates greater than 4 mm/yr or that have ruptured historically), incorporating a greater range of recurrence-time distributions

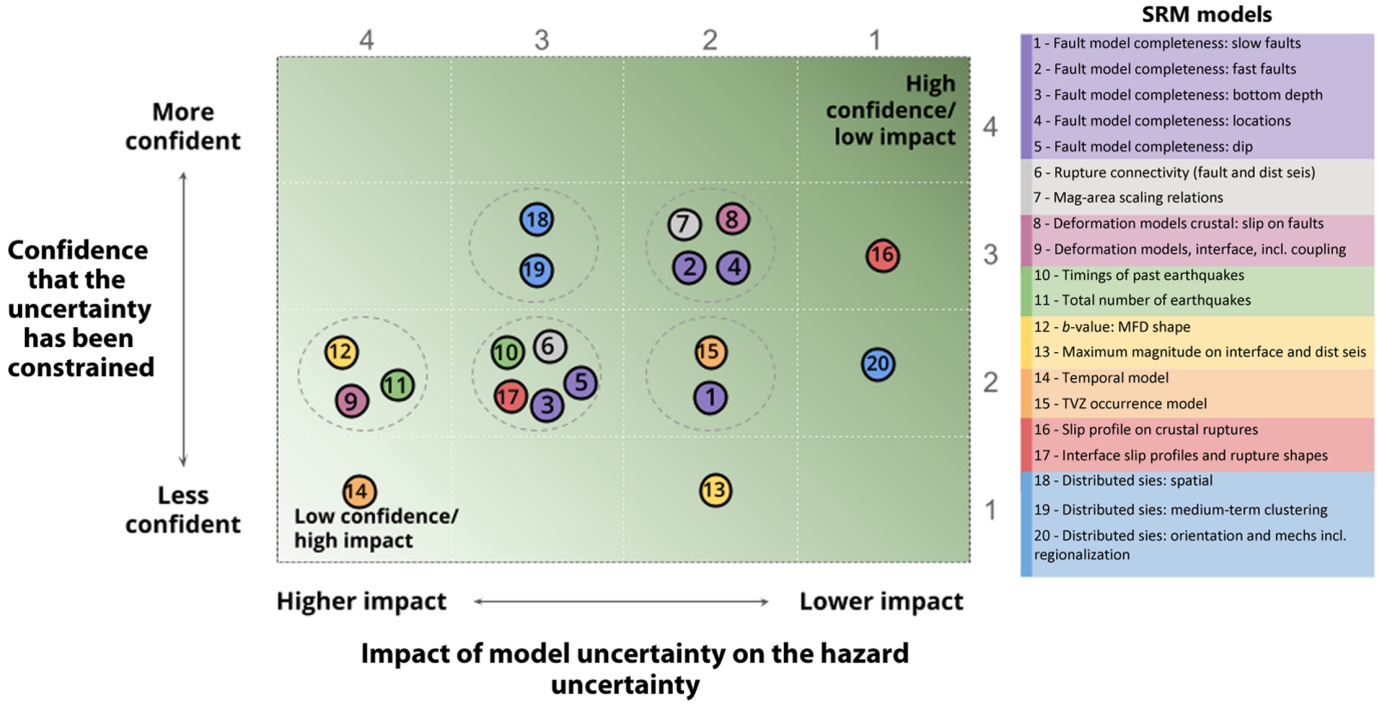

Figure 18. A simplified figure aiming to communicate the confidence the modeling team has in key model parameters and assumptions, and how much the parameters may impact the distribution of hazard. This is a simplified figure that has been used for communicating confidence to end users of the NSHM. Shown is the confidence that a particular uncertainty has been constrained versus the potential impact of the uncertainty on the spread (i.e., distribution) of the hazard. For example, a parameter for which there is relatively high confidence that the uncertainty is constrained and is also considered to have lower impact on the distribution of hazard is considered "More constrained." The assessment indicates that 14: Temporal model (e.g., the overall statistical model for the rate of earthquake occurrence) is shown to be the least constrained. The dashed circles represent groupings of parameters that can be considered equally constrained. The darker green shading indicates parameters in which the uncertainty is relatively more well constrained and impactful. The gray numbers correspond to the respective qualitative scales of more or less confidence and impact. The color version of this figure is available only in the electronic edition.

(e.g., lognormal, Weibel, Gamma, and not just Brownian Passage Time), accommodating uncertainty in paleoearthquake last event timings, entertaining a greater range of recurrence interval aperiodicities, and exploring the impact of magnitude-dependent aperiodicities (especially with regards to assigning the lowest aperiodicities to the largest and, paradoxically, the most complex ruptures).

- The largest uncertainty in the SRM was identified as the MFD. This encompasses both the overall rate (N-value) and the b-value. Significant work was done in the 2022 NZ NSHM revision to constrain these parameters; however, both the aspects remain challenging. Future work should explore improved statistical frameworks and relocations (i.e., location, magnitudes, and tectonic types) of the entire GeoNet catalog. In addition, the polygon-based method for combining the IFM and DSM and determining the MFD for the IFM contains unexplored sensitivities (e.g., polygon width).
- Equally critical to the MFD is the variability in forecast rate. The NZ NSHM 2022 has identified that the standard Poisson assumption is insufficient to capture the range in variability seen in the NZ catalog, and that standard methods do not capture the standard error or bias in the observed mean rate as seen in New Zealand. The NZ NSHM 2022 handles the overdispersion with two independent methods. Future work is required to improve the constraints on this variability and to explore alternative models, such as a negative binomial hazard calculation for the entire model, not just the URZ.

Interface Models

- For both the Hikurangi–Kermadec and the Puysegur subduction interfaces, the deformation model constraints are data-poor. In both cases, the ability to constrain the coupling coefficient is limited and represents a significant source of uncertainty for hazard estimates. In the NZ NSHM 2022 coupling coefficient uncertainty was modeled by accounting for a range of coupling in the assumed N-scaling logic tree branches. The uncertainty in the slip rate and coupling increases for the Kermadec portion of the Hikurangi–Kermadec interface; however, the hazard implications of this portion of the trench are lesser than for the Hikurangi portion. Future work is required to better constrain slip rates on both the interfaces. In addition, there is uncertainty regarding both the shapes of the interface, including its down-dip and up-dip extents of rupture.
- Our ability to constrain the MFDs on both the Hikurangi portion of the Hikurangi–Kermadec interface and the Puysegur

interface is limited by a noticeable paucity of data. For the NZ NSHM 2022, the Hikurangi–Kermadec MFD was modeled using regional constraints that jointly fit both the Hikurangi and the Kermadec portion; this means the MFD was dominated by the *b*-value of the highly productive Kermadec interface, and we were reliant on the slip-rate distribution to constrain a credible MFD on the Hikurangi. This has produced earthquake occurrence rates that are consistent with the deformation models and with the limited paleotsunami data we have. Future work is required to improve both the MFD and the timing and size constraints on past earthquakes.

- The smallest rupture considered on the Hikurangi–Kermadec interface was 30 km × 30 km. This limits the minimum magnitude considered in the IFM to be $\sim M_w$ 7.5; smaller magnitudes were modeled within the DSM. Future improvements in the efficiency of the calculations may allow for the use of smaller patch sizes and the ability to model smaller magnitudes in the IFM. In addition, this may allow for the consideration of additional aspect ratios over the range of rectangular ruptures that were modeled in the NZ NSHM 2022; the importance of this for hazard estimates is unknown.
- Similar improvements to the inversion simulated annealing method as were discussed for the crustal IFM should be considered. In addition, the interface IFM method did not balance the relative uncertainties in the MFD and deformation models as was done for the crustal model; however, as discussed, the constraints on these uncertainties are poor for the interface models due to a lack of data, and future work is required to better constrain these uncertainties.

Slab Model

- Similar to the crustal and interface models, the ability to constrain the slab *b*-value and *N*-value was limited by a paucity of data. To produce robust MFD statistics a uniform rate model was used for both the Hikurangi–Kermadec and Puysegur slab models. Future work may be able to better constrain the MFDs and identify regional variations in the MFDs used. In addition, increased efficiency in calculations may allow for including more MFD-related epistemic uncertainty in the logic tree.

SUMMARY, CONCLUSIONS, AND TRIMMED LOGIC TREE

We have presented the development of the SRM for the NZ NSHM 2022. The details of the components of the DSM and IFM, and how these components are brought together for the final hazard calculations have been explained. The revision incorporates fundamental revisions of all datasets and components of the model. Significant changes include a focus on the total occurrence rate uncertainty and considerations of the implications for the forecast time window; this results in a shift to a 100-year forecast that also acknowledges the uses of the forecasts. We have also implemented an inversion-based fault model for the complex New Zealand network of faults, including application of the method to subduction interfaces for the first time, and incorporated geodetic data into the upper-plate IMF via a compelling method that inverts strain rate for fault-slip rate. We have also applied a hybrid DSM that includes the influence of multiple datasets and provides a credible forecast for all magnitudes. Finally, we have developed a non-Poisson model for lower seismicity zones, acknowledging the large variability in rate observed in these regions.

Based on extensive sensitivity testing in the earthquake occurrence rate space (some of which is presented in the many subarticles of this article), a logic tree has been proposed and used in the NZ NSHM 2022 (Gerstenberger, Bora, *et al.*, 2022; Gerstenberger *et al.*, 2024). Furthermore, based on additional sensitivity in hazard space, with considerations for risk, the logic tree has been further reduced. This additional reduction is to improve computational efficiency and remove unnecessary complexity. Figures 1–3 show the final trimmed logic trees, respectively, for the crustal, interface, and slab models. Gerstenberger, Bora, *et al.* (2022); Gerstenberger *et al.* (2024) detail explorations of the hazard results from the NZ NSHM 2022.

DATA AND RESOURCES

All data used in this article came from the published sources listed in the references except the final hazard calculations. All hazard data can be available at nshm.gns.cri.nz (last accessed December 2023). The supplemental material provides details of the implications of using the minimum magnitude of 6.8 versus 6.9 in the inversion fault model (IFM).

DECLARATION OF COMPETING INTERESTS

The authors acknowledge that there are no conflicts of interest recorded.

ACKNOWLEDGMENTS

The authors would like to thank The National Seismic Hazard Model (NSHM) Technical Advisory Group, which provided technical oversight to the development of all components of the New Zealand (NZ) NSHM attending meetings at all times of the day and night during COVID times: Trevor Allen, Gail Atkinson, Rowan Ballagh, Philip Conway, Ken Elwood, Ned Field, Delphine Fitzenz, Andreas Giannakogiorgos, Tony Holden, Nick Horspool, Nico Luco, Marco Pagani, Linda Poland, Reza Sedgh, Peter Stafford, Mike Stannard, John Townend, and Rick Wentz. The authors also thank Alex Hatem, Richard Briggs, and an anonymous reviewer, who all provided very helpful reviews and comments to greatly improve this article. This work was funded by the New Zealand Ministry of Business, Innovation, and Employment to GNS Science via the National Seismic Hazard Model 2022 Revision Project (Contract Number 2020-BD101).

REFERENCES

Aki, K. (1966). Generation and propagation of G waves from the Niigata earthquake of June 14, *Bull. Earthq. Res. Inst.* **44,** 73–88.

Beavan, J., L. Wallace, N. Palmer, P. Denys, S. Ellis, N. Fournier, S. Hreinsdottir, C. Pearson, and M. Denham (2016). New Zealand GPS velocity field: 1995-2013, *New Zeal. J. Geol. Geophys.* doi: 10.1080/00288306.2015.1112817.

Christophersen, A., N. Litchfield, K. Berryman, R. Thomas, R. Basili, L. Wallace, W. Ries, G. P. Hayes, K. M. Haller, and T. Yoshioka, *et al.* (2015). Development of the Global Earthquake Model's neotectonic fault database, *Nat. Hazards* **79,** 111–135, doi: 10.1007/s11069-015-1831-6.

Biasi, G. (2013). Maximum likelihood recurrence intervals for California paleoseismic sites, *The Uniform California Earthquake Rupture Forecast, UCERF3*, Appendix H, available at https://pubs.usgs.gov/of/2013/1165/ (last accessed December 2023).

Biasi, G., R. Langridge, K. Berryman, K. J. Clark, and U. Cochran (2015). Maximum-likelihood recurrence parameters and conditional probability of a ground-rupturing earthquake on the southern Alpine fault, South Island, New Zealand, *Bull. Seismol. Soc. Am.* **105,** no. 1, 94–106.

Bradley, B. (2013). A New Zealand-specific pseudospectral acceleration ground-motion prediction equation for active shallow crustal earthquakes based on foreign models, *Bull. Seismol. Soc. Am.* **103,** no. 3, 1801–1822.

Bradley, B., S. Bora, R. Lee, E. Manea, M. Gerstenberger, P. Stafford, G. Atkinson, G. Weatherill, J. Hutchinson, C. de la Torre, *et al.* (2024). Summary of the ground-motion characterisation model for the 2022 New Zealand National Seismic Hazard Model, *Bull. Seismol. Soc. Am.*

Bradley, B. A., S. Bora, R. L. Lee, E. F. Manea, M. C. Gerstenberger, P. J. Stafford, G. M. Atkinson, G. Weatherill, J. Hutchinson, and C. A. de la Torre (2022). *Summary of the Ground-Motion Characterisation Model for the 2022 New Zealand National Seismic Hazard Model*, GNS Science, Lower Hutt, New Zealand.

Christophersen, A., and M. Gerstenberger (2024). Expert Judgment in the 2022 Aotearoa New Zealand National Seismic Hazard Model, *Seismol. Res. Lett.*

Christophersen, A., S. Bourguignon, D. Rhoades, T. Allen, J. Salichon, J. Ristau, J. Rollins, and M. Gerstenberger (2022). *Consistent Magnitudes Over Time for the Revision of the New Zealand National Seismic Hazard Model, GNS Science*, GNS Science, Lower Hutt, New Zealand, 68.

Christophersen, A., S. Bourguignon, D. Rhoades, T. Allen, J. Salichon, J. Ristau, J. Rollins, and M. Gerstenberger (2024). Consistent magnitudes over time for the revision of the New Zealand National Seismic Hazard Model, *Bull. Seismol. Soc. Am.* 68.

Coffey, G. L., C. Rollins, R. J. Van Dissen, D. A. Rhoades, K. K. S. Thingbaijam, K. J. Clark, M. C. Gerstenberger, N. J. Litchfield, and A. Nicol (2022). New Zealand National Seismic Hazard Model 2022: Earthquake recurrence derivation from paleoseismic data and probability of detection, *GNS Science report 2022/32*, GNS Science, Lower Hutt, New Zealand, 55, doi: 10.21420/2YWK-ZE30.

Coffey, G., C. Rollins, R. Dissen, D. Rhoades, K. Thingbaijam, M. Gerstenberger, and N. Litchfield (2024). Paleoseismic earthquake recurrence interval derivation for the 2022 revision of the New Zealand National Seismic Hazard Model, *Seismol. Res. Lett.*

Di Giacomo, D., E. Engdahl, and D. Storchak (2018). The ISC-GEM earthquake catalogue (1904-2014): Status after the extension project, *Earth Syst. Sci. Data* **10,** 1877–1899.

Edbrooke, S., D. Heron, P. Forsyth, R. Jongens, and Compilers (2014). *Geological Map of New Zealand 1:1,000,000: Digital Vector Data 2014*, GNS Science, Lower Hutt, New Zealand.

Ellis, S., S. Bannister, R. Dissen, D. Eberhart-Phillips, C. Boulton, M. Reyners, R. Funnell, N. Mortimer, and P. Upton (2022). *New Zealand Fault Rupture Depth Model v1.0: A Provisional Estimate of the Maximum Depth of Seismic Rupture on New Zealand's Active Faults, GNS Science Report*, GNS Science, Lower Hutt, New Zealand, 47.

Ellis, S., S. Bannister, R. Dissen, D. Eberhart-Phillips, C. Boulton, M. Reyners, R. Funnell, N. Mortimer, and P. Upton (2024). New Zealand Fault Rupture Depth Model v.1.0: A provisional estimate of the maximum depth of seismic rupture on New Zealand's active faults, *Bull. Seismol. Soc. Am.*

Evison, F., and D. Rhoades (2004). Demarcation and scaling of long-term seismogenesis, *Pure Appl. Geophys.* **161,** 21–45.

Fayyad, U., and K. Irani (1993). Multi-interval discretization of continuous-valued attributes for classification learning, *Proc. of the 13th International Joint Conference on Artificial Intelligence*, Chambéry, 28 August–3 September 1993, 1022–1027.

Field, E., R. Arrowsmith, G. Biasi, P. Bird, T. Dawson, K. Felzer, D. Jackson, K. Johnson, T. Jordan, C. Madden, *et al.* (2014). Uniform California earthquake rupture forecast, version 3 (UCERF3)-The time-independent model, *Bull. Seismol. Soc. Am.* **104,** no. 3, 1122–1180.

Field, E., G. Biasi, P. Bird, T. Dawson, K. Felzer, D. Jackson, K. Johnson, T. Jordan, and C. Madden (2015). Long-term time-dependent probabilities for the Third Uniform California Earthquake Rupture Forecast (UCERF3), *Bull. Seismol. Soc. Am.* **105,** no. 2A, 511–543.

Field, E., G. Biasi, P. Bird, T. Dawson, K. Felzer, D. Jackson, K. Johnson, T. Jordan, C. Madden, and A. Michael (2013). Uniform California Earthquake Rupture Forecast, (UCERF3)-The Time Independent Model, *U.S. Geol. Surv.*, available at https://pubs.usgs.gov/of/2013/1165/ (last accessed December 2023).

Field, E., K. Milner, and N. Luco (2022). The seismic hazard implications of declustering and Poisson assumptions inferred from a fully time-dependent model, *Bull. Seismol. Soc. Am.* **112,** no. 1, 527–537.

Fletcher, J., M. Oskin, and O. Teran (2016). The role of a keystone fault in triggering the complex El Mayor–Cucapah earthquake rupture, *Nature Geosci.* **9,** no. 4, 303–307.

Frankel, A. (1995). Mapping seismic hazard in the central and eastern United States, *Seismol. Res. Lett.* **66,** no. 4, 8–21, doi: 10.1785/gssrl.66.4.8.

Gardner, J., and L. Knopoff (1974). Is the sequence of earthquakes in southern California, with aftershocks removed, Poissonian? *Bull. Seismol. Soc. Am.* **64,** no. 5, 1363–1367.

Gerstenberger, M., and D. Rhoades (2010). New Zealand earthquake forecast testing centre, in *Seismogenesis and Earthquake Forecasting: The Frank Evison*, M. Savage, D. Rhoades, E. Smith, M. Gerstenberger, and D. Vere-Jones (Editors), Vol. II, Pageoph Topical Volumes, Springer, Basel.

Gerstenberger, M., S. Bora, B. Bradley, C. DiCaprio, A. Kaiser, E. Manea, A. Nicol, C. Rollins, M. Stirling, K. Thingbaijam, *et al.* (2024). The 2022 New Zealand National Seismic Hazard Model: Process, overview and results, *Bull. Seismol. Soc. Am.* doi: 10.1785/0120230182.

Gerstenberger, M. C., S. Bora, B. A. Bradley, C. DiCaprio, R. J. Van Dissen, G. M. Atkinson, C. Chamberlain, A. Christophersen, K. J.

Clark, G. L. Coffey, *et al.* (2022). The 2022 New Zealand National Seismic Hazard Model: Model, hazard and process overview, *GNS Science Report 2022/57*, GNS Science, Lower Hutt, New Zealand, 106, doi: 10.21420/TB83-7X19.

Gerstenberger, M., W. Marzocchi, T. Allen, M. Pagani, J. Adams, L. Danciu, E. Field, H. Fujiwara, N. Luco, K.-F. Ma, *et al.* (2020). Probabilistic seismic hazard analysis at regional and national scales: State of the art and future challenges, *Rev. Geophys.* **58,** 000,653.

Gerstenberger, M. C., D. A. Rhoades, and G. H. McVerry (2016). A hybrid time-dependent probabilistic seismic-hazard model for Canterbury, New Zealand, *Seismol. Res. Lett.* **87,** no. 6, 1311–1318.

Gerstenberger, M. C., R. J. Van Dissen, C. Rollins, C. DiCaprio, C. Chamberlain, A. Christophersen, G. L. Coffey, S. M. Ellis, P. Iturrieta, K. M. Johnson, *et al.* (2022). The seismicity rate model for the 2022 New Zealand National Seismic Hazard Model, *GNS Science report 2022/47*, GNS Science, Lower Hutt, New Zealand, doi: 10.21420/2EXG-NP48.

Griffin, J., T. Allen, and M. Gerstenberger (2020). Seismic hazard assessment in Australia: can structured expert elicitation achieve consensus in the "land of the fair go"? *Seismol. Res. Lett.* **91,** 859–873.

Griffin, J., M. Stirling, K. Wilcken, and D. Barrell (2022). Late Quaternary slip rates for the Hyde and Dunstan faults, southern New Zealand: Implications for strain migration in a slowly deforming continental plate margin, *Tectonics* **41,** doi: 10.1029/2022TC007250.

Grünthal, G. (1985). The up-dated earthquake catalogue for the German Democratic Republic and adjacent areas–statistical data characteristics and conclusions for hazard assessment, in *3rd International Symposium on the Analysis of Seismicity and Seismic Risk*, 17–22 June 1985, Liblice, Czechoslovakia, Geophysical Institute of the Czechoslovak Academy of Sciences, Prague, Czech Republic, 19–25.

Haines, A. (1981a). A local magnitude scale for New Zealand earthquakes, *Bull. Seismol. Soc. Am.* **71,** no. 1, 275–294.

Haines, A. (1981b). Systematic effects of the introduction in 1977 of a new magnitude scale for New Zealand earthquakes, *New Zeal. J. Geol. Geophys.* **24,** no. 2, 141–153.

Haines, A., and L. Wallace (2020). New Zealand-wide geodetic strain rates using a physics-based approach, *Geophys. Res. Lett.* **47,** doi: 10.1029/2019GL084606.

Haines, A., L. Dimitrova, L. Wallace, and C. Williams (2015). *Enhanced Surface Imaging of Crustal Deformation: Obtaining Tectonic Force Fields Using GPS Data*, Springer International Publishing AG, Switzerland.

Hanks, T., and H. Kanamori (1979). A moment magnitude scale, *J. Geophys. Res.* **84,** no. 5, 2348–2350.

Hayes, G., G. Moore, D. Portner, M. Hearne, H. Flamme, M. Furtney, and G. Smoczyk (2018). Slab2, a comprehensive subduction zone geometry model, *Science* **362,** no. 6410, 58–61.

Helmstetter, A., and M. Werner (2012). Adaptive spatiotemporal smoothing of seismicity for long-term earthquake forecasts in California, *Bull. Seismol. Soc. Am.* **102,** no. 6, 2518–2529.

Iturrieta, P., M. Gerstenberger, C. Rollins, R. Dissen, T. Wang, and D. Schorlemmer (2022). *Accounting for Earthquake Rates' Temporal and Spatial Uncertainties through Least-Information Forecasts, GNS Science Report*, GNS Science, Lower Hutt, New Zealand, 38.

Iturrieta, P., M. Gerstenberger, C. Rollins, R. Van Dissen, T. Wang, and D. Schorlemmer (2024a). Accounting for earthquake rates' temporal and spatial uncertainties through least-information forecasts, *Bull. Seismol. Soc. Am.* doi: 10.1785/0120230164.

Iturrieta, P., M. Gerstenberger, J. Rollins, R. Van Dissen, T. Wang, and D. Schorlemmer (2024b). Implementing non-Poissonian forecasts of distributed seismicity to the New Zealand Seismic Hazard Model 2022, *Bull. Seismol. Soc. Am.* doi: 10.1785/0120230168.

Johnson, K., L. Wallace, J. Maurer, I. Hamling, C. Williams, C. Rollins, M. Gerstenberger, and R. Dissen (2022). *Geodetic Deformation Model for the 2022 Update of the New Zealand National Seismic Hazard Model, GNS Science Report*, GNS Science, Lower Hutt, New Zealand.

Johnson, K., L. Wallace, J. Maurer, I. Hamling, C. Williams, C. Rollins, M. Gerstenberger, and R. Dissen (2024). Geodetic deformation model for the 2022 update of the New Zealand National Seismic Hazard Model, *J. Geophys. Res.*

Kolaj, M., J. Adams, and S. Halchuk (2020). The 6th generation Seismic Hazard Model of Canada, *17th World Conference on Earthquake Engineering, 17WCEE 2020*, Sendai, Japan, 13–18 September 2018.

Kurushin, R., A. Bayasgalan, M. Ölziybat, B. Enkhtuvshin, P. Molnar, C. Bayarsayhan, K. Hudnut, and J. Lin (1997). *The Surface Rupture of the 1957 Gobi-Altay, Mongolia, Earthquake*, Geological Society of America, Special Paper 320, 143, available at https://books.google.com/books?hl=en&lr=&id=XCwnBIjEmmMC&oi=fnd&pg=PP5&dq=The+surface+rupture+of+the+1957+Gobi%E2%80%90Altay,+Mongolia,+earthquake&ots=SWbWItRxY5&sig=wVZjxnktUg5cKAX68b-QFlos0bE (last accessed December 2023).

Litchfield, N., R. Dissen, R. Sutherland, P. Barnes, S. Cox, R. Norris, R. Beavan, R. Langridge, P. Villamor, and K. Berryman (2014). A model of active faulting in New Zealand. *New Zeal. J. Geol. Geophys.* **57,** no. 1, 32–56.

Litchfield, N., J. Humphrey, R. Morgenstern, R. Langridge, G. Coffey, and R. Dissen (2022). New Zealand Paleoseismic Site Database: data dictionary, *GNS Science report 2021/40*, GNS Science, Lower Hutt, New Zealand, 42 pp., doi: 10.21420/G5K4-ES33.

Litchfield, N., J. Humphrey, R. Morgenstern, R. Langridge, G. Coffey, and R. Van Dissen (2024). The New Zealand paleoseismic site database—version 1.0, *Seismol. Res. Lett.* doi: 10.1785/0220230150.

Litchfield, N., P. Villamor, R. Dissen, A. Nicol, P. Barnes, D. Barrell, J. Pettinga, R. Langridge, T. Little, and J. Mountjoy (2018). Surface rupture of multiple crustal faults in the 2016 M_w 7.8 Kaikoura, New Zealand, earthquake, *Bull. Seismol. Soc. Am.* **108,** no. 3B, 1496–1520.

Madden, C., D. Haddad, J. Salisbury, O. Zielke, R. Arrowsmith, J. Colunga (2013). Compilation of slip-in-the-last-event data and analysis of last event, repeated slip, and average displacement for recent and prehistoric ruptures, in *The Uniform California Earthquake Rupture Forecast, Version 3 (UCERF3) - the Time-Independent Model, USGS Open-File Report 2013-1165*, E. H. Field, G. P. Biasi, P. Bird, T. E. Dawson, K. R. Felzer, D. D. Jackson, K. M. Johnson, T. H. Jordan, C. Madden, and A. J. Michael, *et al.* (Editors), U.S. Geological Survey, Reston, Virginia, U.S.A.

Marzocchi, W., M. Taroni, and J. Selva (2015). Accounting for epistemic uncertainty in PSHA: Logic tree and ensemble modeling, *Bull. Seismol. Soc. Am.* **105,** no. 4, 2151–2159.

Maurer, J., K. Johnson, L. Wallace, I. Hamling, C. Williams, C. Rollins, M. Gerstenberger, and R. Van Dissen (2024). Geodetic strain rates for the 2022 update of the New Zealand National Seismic Hazard Model, *Bull. Seismol. Soc. Am.* doi: 10.1785/0120230145.

Meletti, C., W. Marzocchi, V. D'amico, G. Lanzano, L. Luzi, F. Martinelli, B. Pace, A. Rovida, M. Taroni, F. Visini, *et al.* (2021). The new Italian seismic hazard model (MPS19), *Ann. Geophys.* **64,** no. 1, doi: 10.4401/ag-8579.

Milner, K., and E. Field (2023). A comprehensive fault system inversion approach: Methods and application to NSHM23, *Bull. Seismol. Soc. Am.* doi: 10.1785/0120230122.

Milner, K., M. Page, E. Field, T. Parsons, G. Biasi, and B. Shaw (2013). Appendix T–Defining the inversion rupture set using plausibility filters, *Uniform California Earthquake Rupture Forecast*, available at https://pubs.usgs.gov/of/2013/1165/ (last accessed December 2023).

Milner, K., B. Shaw, and E. Field (2022). Enumerating plausible multifault ruptures in complex systems with physical constraints, *Bull. Seismol. Soc. Am.*

Mortimer, N., B. Smith Lyttle, and J. Black (2020). *Te Riu-a-Māui/Zealandia digital geoscience data compilation, GNS Science geological map 11, 1: 8 500 000*, GNS Science, Lower Hutt, New Zealand, available at https://data.gns.cri.nz/tez/index.html?content=/mapservice/Content/Zealandia/StartHere.html (last accessed December 2023).

Nicol, A., R. Van Dissen, M. Stirling, and M. Gerstenberger (2016). Completeness of the paleoseismic active-fault record in New Zealand, *Seismol. Res. Lett.* **87,** no. 6, 1299–1310.

Nicol, A., J. Khajavi, J. Humphrey, R. Van Dissen, M. Gerstenberger, and M. Stirling (2022). Geometries and slip of historical surface-rupturing earthquakes in New Zealand and their application to seismic hazard analysis, *EQC 16/718*, available at https://www.eqc.govt.nz/resilience-and-research/research/search-all-research-reports/negeometries-and-slip-of-historical-surface-rupturing-earthquakes-in-new-zealand-and-their-application-to-seismic-hazard-analysisw-document-page/ (last accessed December 2023).

Nicol, A., R. Robinson, R. Van Dissen, and A. Harvison (2016). Variability of recurrence interval and single-event slip for surface-rupturing earthquakes in New Zealand, *New Zeal. J. Geol. Geophys.* **59,** no. 1, 97–116.

Pagani, M., K. Johnson, and J. Garcia Pelaez (2021). Modelling subduction sources for probabilistic seismic hazard analysis, *Geol. Soc. Lond.* **501,** no. 1, 225–244.

Pagani, M., D. Monelli, G. Weatherill, L. Danciu, H. Crowley, V. Silva, P. Henshaw, L. Butler, M. Nastasi, L. Panzeri, *et al.* (2014). OpenQuake engine: An open hazard (and risk) software for the global earthquake model, *Seismol. Res. Lett.* **85,** no. 3, 692–702.

Page, M., E. Field, K. Milner, and P. Powers (2013). Appendix N-grand inversion implementation and testing, *Geol. Surv. Open-File Rept.*

Page, M., E. Field, K. Milner, and P. Powers (2014). The UCERF3 grand inversion: Solving for the long-term rate of ruptures in a fault system, *Bull. Seismol. Soc. Am.* **104,** no. 3, 1181–1204.

Petersen, M., A. Shumway, P. Powers, E. Field, M. Moschetti, K. Jaiswal, K. Milner, S. Razaeinan, A. Frankel, A. Llenos, *et al.* (2023). The 2023 U.S. 50-State National Seismic Hazard Model: Overview and implications, *Earthq. Spectra* (in review).

Power, W., L. Wallace, X. Wang, and M. Reyners (2012). Tsunami hazard posed to New Zealand by the Kermadec and southern New Hebrides subduction margins; an assessment based on plate boundary kinematics, interseismic coupling, and historical seismicity, *Pure Appl. Geophys.* **169,** 1–36.

Powers, P., and E. Field (2013). Appendix O: Gridded seismicity sources, *U.S. Geol. Surv. Open-File Rept. 2013-1165-O*, available at https://pubs.usgs.gov/of/2013/1165/ (last accessed December 2023).

Ramírez-Gallego, S., S. García, H. Mouriño-Talín, D. Martínez-Rego, V. Bolón-Canedo, A. Alonso-Betanzos, J. Benítez, and F. Herrera (2016). Data discretization: Taxonomy and big data challenge, *Wiley Interdiscip. Rev.* **6,** no. 1, 5–21.

Rastin, S. J., D. A. Rhoades, C. Rollins, M. C. Gerstenberger, A. Christophersen, and K. K. S. Thingbaijam (2022). Spatial distribution of earthquake occurrence for the New Zealand National Seismic Hazard Model revision, *GNS Science report 2021/51*, GNS Science, Lower Hutt, New Zealand, doi: 10.21420/YKQ8-1C41.

Rastin, S., D. Rhoades, C. Rollins, M. Gerstenberger, and A. Christophersen (2024). Spatial distribution of earthquake occurrence for the New Zealand National Seismic Hazard Model revision, *Bull. Seismol. Soc. Am.*

Rastin, S., D. Rhoades, J. Rollins, and M. Gerstenberger (2024). Estimation of uncertainty in the earthquake rate, *Seismol. Res. Lett.* doi: 10.1785/0220230242.

Rastin, S. J., D. A. Rhoades, and A. Christophersen (2021). Space-time trade-off of precursory seismicity in New Zealand and California revealed by a medium-term earthquake forecasting model, *Appl. Sci.* **11,** no. 21, 10,215.

Rattenbury, M. (2022). *Regional Fault Orientation and Length Analysis, Aotearoa New Zealand*, GNS Science, Lower Hutt, New Zealand, 49.

Reasenberg, P. (1985). Second-order moment of central California seismicity, 1969-1982, *J. Geophys. Res.* **90,** no. B7, 5479–5495.

Rhoades, D., and A. Christophersen (2017). Magnitude conversion of earthquake rate forecasts, *Bull. Seismol. Soc. Am.* **107,** no. 6, 3037–3043.

Rhoades, D., and A. Christophersen (2019). Time-varying probabilities of earthquake occurrence in central New Zealand based on the EEPAS model compensated for time-lag, *Geophys. J. Int.* **219,** no. 1, 417–429.

Rhoades, D., and R. Dissen (2003). Estimates of the time-varying hazard of rupture of the Alpine fault, New Zealand, allowing for uncertainties, *New. Zeal. J. Geol. Geophys.* **46,** no. 4, 479–488.

Rhoades, D., and F. Evison (2005). Test of the EEPAS forecasting model on the Japan earthquake catalogue, *Pure Appl. Geophys.* **162,** 1271–1290.

Rhoades, D. A., and F. F. Evison (2004). Long-range earthquake forecasting with every earthquake a precursor according to scale, *Pure Appl. Geophys.* **161,** 47–72.

Rhoades, D., A. Christophersen, S. Bourguignon, J. Ristau, and J. Salichon (2020). A depth-dependent local magnitude scale for New Zealand earthquakes consistent with moment magnitude, *Bull. Seismol. Soc. Am.* **111,** no. 2, 1056–1066.

Rhoades, D., R. Van Dissen, R. Langridge, T. Little, D. Ninis, E. Smith, and R. Robinson (2011). Re-evaluation of conditional probability of rupture of the Wellington-Hutt Valley segment of the Wellington fault, *Bull. New Zeal. Soc. Earthq. Eng.*

Rhoades, D., M. Liukis, A. Christophersen, and M. Gerstenberger (2016). Retrospective tests of hybrid operational earthquake forecasting models for Canterbury, *Geophys. J. Int.* **204,** no. 1, 440–456.

Rhoades, D., D. Schorlemmer, M. Gerstenberger, A. Christophersen, J. Zechar, and M. Imoto (2011). Efficient testing of earthquake forecasting models, *Acta Geophys.* **59,** 728–747.

Richter, C. (1935). An instrumental earthquake magnitude scale, *Bull. Seismol. Soc. Am.* **25,** no. 1, 1–32.

Ristau, J. (2013). Update of regional moment tensor analysis for earthquakes in New Zealand and adjacent offshore regions, *Bull. Seismol. Soc. Am.* **103,** no. 4, 2520–2533.

Rollins, C., A. Christophersen, K. Thingbaijam, M. Gerstenberger, J. Hutchinson, D. Eberhart-Phillips, S. Bannister, J. Townend, R. Van Dissen, S. Rastin, *et al.* (2024). An integrated earthquake catalogue for Aotearoa New Zealand (version 1) and its implications for earthquake rates: 1. Catalogue assembly, seismological regime classifications, and depth distributions, *Bull. Seismol. Soc. Am.*

Rollins, C., M. Gerstenberger, D. Rhoades, S. Rastin, A. Christophersen, K. Thingbaijam, R. Dissen, and T. Wang (2024). An integrated earthquake catalogue for Aotearoa New Zealand (version 1) and its implications for earthquake rates: 2. Magnitude-frequency distributions, *Bull. Seismol. Soc. Am.*

Rollins, C., D. A. Rhoades, S. J. Rastin, M. C. Gerstenberger, A. Christophersen, K. K. S. Thingbaijam, R. J. Van Dissen, K. Graham, and J. Fraser (2022). The magnitude-frequency distributions of earthquakes in the greater New Zealand region and along the Hikurangi-Kermadec and Puysegur subduction zones, and their uncertainties, with application to the 2022 New Zealand National Seismic Hazard Model, *GNS Science report 2022/48*, GNS Science, Lower Hutt, New Zealand, 77 pp., doi: 10.21420/SXPX-8C68.

Rollins, C., K. Thingbaijam, J. Hutchinson, M. Gerstenberger, A. Christophersen, D. Eberhart-Phillips, S. Rastin, and R. Dissen (2021). *A Combined New Zealand Earthquake Catalogue, Event Classifications, and Models of the Depth Distribution of Shallow Earthquakes in the Greater New Zealand region, Technical Report*, GNS Science, Lower Hutt, New Zealand.

Sandwell, D., and P. Wessel (2016). Interpolation of 2-D vector data using constraints from elasticity, *Geophys. Res. Lett.* **43,** no. 20, 10,703–10,709.

Seebeck, H., R. J. Van Dissen, N. J. Litchfield, P. M. Barnes, A. Nicol, R. M. Langridge, D. J. A. Barrell, P. Villamor, S. M. Ellis, M. S. Rattenbury, *et al.* (2022). New Zealand Community Fault Model–version 1.0, *GNS Science report 2021/57*, GNS Science, Lower Hutt, New Zealand, 97 pp., doi: 10.21420/GA7S-BS61.

Seebeck, H., R. Dissen, N. Litchfield, P. Barnes, A. Nicol, R. Langridge, D. Barrell, P. Villamor, S. Ellis, M. Rattenbury, *et al.* (2023). New Zealand Community Fault Model–version 1.0: An improved geological foundation for seismic hazard modeling, *New Zeal. J. Geol. Geophys.*

Shaw, B. (2013). Earthquake surface slip-length data is fit by constant stress drop and is useful for seismic hazard analysis, *Bull. Seismol. Soc. Am.* **103,** no. 2A, 876–893.

Shaw, B., B. Fry, A. Nicol, A. Howell, and M. Gerstenberger (2022). An earthquake simulator for New Zealand, *Bull. Seismol. Soc. Am.* **112,** no. 2, 763–778.

Stafford, P. (2022). *A Model for the Distribution of Response Spectral Ordinates from New Zealand Crustal Earthquakes Based Upon Adjustments to the Chiou and Youngs (2014) Response Spectral Model*, GNS Science, Lower Hutt, New Zealand.

Stirling, M., T. Goded, K. Berryman, and N. Litchfield (2013). Selection of earthquake scaling relationships for seismic-hazard analysis, *Bull. Seismol. Soc. Am.* **103,** no. 6, 2993–3011.

Stirling, M., G. McVerry, and K. Berryman (2002). A new seismic hazard model of New Zealand, *Bull. Seismol. Soc. Am.* **92,** 1878–1903.

Stirling, M., G. McVerry, M. Gerstenberger, N. Litchfield, R. Dissen, K. Berryman, P. Barnes, L. Wallace, and P. Villamor (2012). National seismic hazard model for New Zealand: 2010 update, *Bull. Seismol. Soc. Am.* **102,** no. 4, 1514–1542.

Stirling, M., B. Shaw, M. Fitzgerald, and C. Ross (2021). Selection and evaluation of magnitude - area scaling relations for update of the New Zealand National Seismic Hazard Model, Dunedin, New Zealand, 49, available at https://nshm.gns.cri.nz/Resources/ScienceReports (last accessed December 2023).

Stirling, M., B. Shaw, M. Fitzgerald, and C. Ross (2024). Selection and evaluation of magnitude - area scaling relations for update of the New Zealand National Seismic Hazard Model, *Seismol. Res. Lett.*

Szu, H., and R. Hartley (1987). Fast simulated annealing, *Phys. Lett. A* **122,** nos. 3/4, 157–162.

Thingbaijam, K., M. Gerstenberger, C. Rollins, A. Christophersen, C. Williams, J. Ristau, S. Rastin, J. Fraser, and R. Dissen (2022). *A Seismogenic Slab Source Model for New Zealand, GNS Science Report*, GNS Science, Lower Hutt, New Zealand, 27.

Thingbaijam, K., M. Gerstenberger, C. Rollins, A. Christophersen, C. Williams, J. Ristau, S. Rastin, J. Fraser, and R. Dissen (2024). A seismogenic slab source model for New Zealand, *Bull. Seismol. Soc. Am.*

Thingbaijam, K., M. Rattenbury, R. Van Dissen, M. Gerstenberger, and J. Ristau (2022). *A Simple Model of Faulting Patterns for Distributed Seismicity in New Zealand, Technical Report 2022/10*, GNS Science, Lower Hutt, New Zealand.

Thingbaijam, K., M. Rattenbury, R. Van Dissen, M. Gerstenberger, J. Ristau, and D. D. Fitzenz (2023). Characterization of focal mechanisms for upper crustal distributed seismicity in Aotearoa New Zealand, *Seismol. Res. Lett.* (accepted).

Van Dissen, R., E. Abbott, R. Zinke, D. Ninis, J. Dolan, T. Little, E. Rhodes, N. Litchfield, and A. Hatem (2020). Slip rate variations on major strike-slip faults in central New Zealand and potential impacts on hazard estimation, *NZSEE 2020 Annual Conference Proceedings*, Wellington, New Zealand, 22–24 April 2020, New Zealand Society for Earthquake Engineering, 8.

Van Dissen, R., D. Rhoades, T. Little, N. Litchfield, R. Carne, and P. Villamor (2013). Conditional probability of rupture of the Wairarapa and Ohariu faults, New Zealand, *New Zeal. J. Geol. Geophys.* **56,** no. 2, 53–67.

Van Dissen, R., H. Seebeck, L. Wallace, C. Rollins, M. Gerstenberger, A. Howell, C. DiCaprio, and C. Williams (2022). *New Zealand National Seismic Hazard Model 2022: Geologic and Subduction Interface Deformation Models, GNS Science Report 2022/31*, GNS Science, Lower Hutt, New Zealand.

Van Dissen, R., H. Seebeck, L. Wallace, C. Rollins, M. Gerstenberger, A. Howell, C. DiCaprio, and C. Williams (2024). New Zealand National Seismic Hazard Model 2022: Geologic and subduction interface deformation models, *Bull. Seismol. Soc. Am.*

Wallace, L., P. Barnes, J. Beavan, R. Dissen, N. Litchfield, J. Mountjoy, R. Langridge, G. Lamarche, and N. Pondard (2012). The kinematics of a transition from subduction to strike-slip: An example from the central New Zealand plate boundary, *J. Geophys. Res.* **117,** no. B2, doi: 10.1029/2011JB008640.

Wallace, L., J. Beavan, R. McCaffrey, K. Berryman, and P. Denys (2007). Balancing the plate motion budget in the South Island, New Zealand using GPS, geological and seismological data, *Geophys. J. Int.* **168,** no. 1, 332–352.

Wallace, L., J. Beavan, R. McCaffrey, and D. Darby (2004). Subduction zone coupling and tectonic block rotations in the North Island, New Zealand, *J. Geophys. Res.* **109,** no. B12, doi: 10.1029/2004JB003241.

Wang, H., and T. Wright (2012). Satellite geodetic imaging reveals internal deformation of western Tibet, *Geophys. Res. Lett.* **39,** 07,303.

Weiss, J. R., R. J. Walters, Y. Morishita, T. J. Wright, M. Lazecky, H. Wang, E. Hussain, A. J. Hooper, J. R. Elliott, C. Rollins, *et al.* (2020). High-resolution surface velocities and strain for Anatolia from Sentinel-1 InSAR and GNSS data, *Geophys. Res. Lett.* **47,** no. 17, 087,376.

Weldon, R., and G. Biasi (2013). Probability of detection of ground rupture at paleoseismic sites, in *The Uniform California Earthquake Rupture Forecast, Version 3 (UCERF3)—the Time-Independent Model Appendix I. (USGS Open-File Report 2013-1165)*, E. H. Field, G. P. Biasi, P. Bird, T. E. Dawson, K. R. Felzer, D. D. Jackson, K. M. Johnson, T. H. Jordan, C. Madden, and A. J. Michael, *et al.* (Editors), U.S. Geological Survey, Reston, Virginia, U.S.A., 26.

Williams, C., D. Eberhart-Phillips, S. Bannister, D. Barker, S. Henrys, M. Reyners, and R. Sutherland (2013). Revised interface geometry for the Hikurangi subduction zone, New Zealand, *Seismol. Res. Lett.* **84,** no. 6, 1066–1073.

Zinke, R., J. Dolan, E. Rhodes, R. Dissen, A. Hatem, C. McGuire, N. Brown, and J. Grenader (2021). Latest Pleistocene-Holocene incremental slip rate of the Wairau fault: Implications for long-distance and long-term coordination of faulting between North and South Island, New Zealand, *Geochem. Geophys. Geosys.* **22,** no. 9, 1525–2027.

AUTHORS AND AFFILIATIONS

Matthew C. Gerstenberger: GNS Science Te Pu Ao, Lower Hutt, New Zealand, https://orcid.org/0000-0002-0392-7114; **Russ Van Dissen:** GNS Science Te Pu Ao, Lower Hutt, New Zealand, https://orcid.org/0000-0001-8224-7573; **Chris Rollins:** GNS Science Te Pu Ao, Lower Hutt, New Zealand, https://orcid.org/0000-0002-5291-6956; **Chris DiCaprio:** GNS Science Te Pu Ao, Lower Hutt, New Zealand, https://orcid.org/0009-0000-5823-0384; **Kiran K. S. Thingbaijim:** GNS Science Te Pu Ao, Lower Hutt, New Zealand, https://orcid.org/0000-0002-2415-2266; **Sanjay Bora:** GNS Science Te Pu Ao, Lower Hutt, New Zealand, https://orcid.org/0000-0002-2043-0513; **Chris Chamberlain:** GNS Science Te Pu Ao, Lower Hutt, New Zealand, https://orcid.org/0009-0002-3582-4555; **Annemarie Christophersen:** GNS Science Te Pu Ao, Lower Hutt, New Zealand, https://orcid.org/0000-0003-1467-1414; **Genevieve L. Coffey:** GNS Science Te Pu Ao, Lower Hutt, New Zealand, https://orcid.org/0000-0002-2938-1359; **Susan M. Ellis:** GNS Science Te Pu Ao, Lower Hutt, New Zealand, https://orcid.org/0000-0002-2754-4687; **Pablo Iturrieta:** GFZ German Research Center for Geoscience, Potsdam, Germany, https://orcid.org/0000-0002-4787-1343; **Kaj M. Johnson:** Indiana University, Bloomington, Indiana, https://orcid.org/0000-0003-1511-5241; **Nicola J. Litchfield:** GNS Science Te Pu Ao, Lower Hutt, New Zealand, https://orcid.org/0000-0002-2053-3176; **Andy Nicol:** University of Canterbury, Chrischurch, New Zealand, https://orcid.org/0000-0001-5181-1151; **Kevin R. Milner:** University of Southern California, Los Angeles, California, U.S.A., https://orcid.org/0000-0002-9118-6378; **Sepi J. Rastin:** GNS Science Te Pu Ao, Lower Hutt, New Zealand, https://orcid.org/0000-0003-1001-3676; **David Rhoades:** GNS Science Te Pu Ao, Lower Hutt, New Zealand, https://orcid.org/0000-0002-9512-9215; **Hann Seebeck:** GNS Science Te Pu Ao, Lower Hutt, New Zealand, https://orcid.org/0000-0002-1749-6626; **Bruce E. Shaw:** Lamont-Doherty Earth Observatory, Columbia University, Palisades, New York, U.S.A., https://orcid.org/0000-0002-6431-9745; **Mark W. Stirling:** University of Otago, Dunedin, New Zealand, https://orcid.org/0000-0002-2562-4675; **Laura Wallace:** GNS Science Te Pu Ao, Lower Hutt, New Zealand University of Texas, Austin, Texas, U.S.A; **Trevor I. Allen:** Geoscience Australia, Canberra, Australia, https://orcid.org/0000-0003-3420-547X; **Brendon A. Bradley:** University of Canterbury, Canterbury, New Zealand, https://orcid.org/0000-0002-4450-314X; **Danielle Charlton:** GNS Science Te Pu Ao, Lower Hutt, New Zealand, https://orcid.org/0000-0002-7837-514X; **Kate J. Clark:** GNS Science Te Pu Ao, Lower Hutt, New Zealand, https://orcid.org/0000-0003-0726-9005; **Jeff Fraser:** WSP, Christchurch, New Zealand; **Jonathan Griffin:** Geoscience Australia, Canberra, Australia, https://orcid.org/0000-0002-5197-1742; **Ian J. Hamling:** GNS Science Te Pu Ao, Lower Hutt, New Zealand, https://orcid.org/0000-0003-4324-274X; **Andy Howell:** GNS Science Te Pu Ao, Lower Hutt, New Zealand University of Canterbury, Canterbury, New Zealand; **Emma Hudson-Doyle:** Massey University, Wellington, New Zealand, https://orcid.org/0000-0002-2878-0972; **Anne Hulsey:** University of Auckland, Auckland, New Zealand, https://orcid.org/0000-0002-4265-055X; **V. Oakley Jurgens:** GNS Science Te Pu Ao, Lower Hutt, New Zealand, https://orcid.org/0009-0007-3335-1711; **Anna E. Kaiser:** GNS Science Te Pu Ao, Lower Hutt, New Zealand, https://orcid.org/0000-0002-0458-5451; **Rachel Kirkman:** GNS Science Te Pu Ao, Lower Hutt, New Zealand; **Rob M. Langridge:** GNS Science Te Pu Ao, Lower Hutt, New Zealand; **Jeremy Maurer:** Missouri University of Science and Technology, Rolla, Missouri, U.S.A., https://orcid.org/0000-0002-3624-5961; **Mark S. Rattenbury:** GNS Science Te Pu Ao, Lower Hutt, New Zealand, https://orcid.org/0000-0003-3270-2675; **John Ristau:** GNS Science Te Pu Ao, Lower Hutt, New Zealand, https://orcid.org/0000-0002-7363-5205; **Danijel Schorlemmer:** GFZ German Research Center for Geoscience, Potsdam, Germany, https://orcid.org/0000-0003-3969-1059; **John Townend:** Victoria University of Wellington, Wellington, New Zealand, https://orcid.org/0000-0002-7017-620X; **Pilar Villamor:** GNS Science Te Pu Ao, Lower Hutt, New Zealand, https://orcid.org/0000-0002-9541-290X; and **Charles Williams:** GNS Science Te Pu Ao, Lower Hutt, New Zealand, https://orcid.org/0000-0001-7435-9196

Manuscript received 6 July 2023
Published online 2 January 2024